Title: The spherical ejecta of AT2017gfo

Speakers: Albert Sneppen

Series: Strong Gravity

Date: April 06, 2023 - 1:00 PM

URL: https://pirsa.org/23040084

Abstract: The geometry of kilonovae is a key diagnostic of the physics of merging neutron stars with current hydrodynamical merger models typically showing aspherical ejecta. Previously, Sr II was identified in the spectrum of the only well-studied kilonova AT2017gfo, associated with the gravitational wave event GW170817. In this talk, we show that combining the strong Sr II P Cygni absorption-emission spectral feature and the blackbody nature of the kilonova spectrum, to determine that the kilonova is highly spherical at early epochs. Line shape analysis combined with the known inclination angle of the source also shows the same sphericity independently. The near-spherical geometry suggests early spectra of kilonovae may provide excellent precision cosmic distance measurements using the Expanding Photosphere Method.

Zoom link: https://pitp.zoom.us/j/97287055430?pwd=bFVyeTRuZHVLcGlDdnhlK1d0OWE1Zz09

DAWN
Visitors to Cosmic Dawn Center (DAWN)

KØBENHAVNS UNIVERSITET

Article

Spherical symmetry in the kilonova AT2017gfo/GW170817

https://www.nature.com/articles/s41586-022-05616-x

April 6th 2023, Strong Gravity Seminar at Perimeter Institute

Albert Sneppen [1,2], Darach Watson [1,2], Andreas Bauswein [3], Oliver Just [3,4], Rubina Kotak [5], Ehud Nakar [6], Dovi Poznanski [6] & Stuart Sim [7]

1) Cosmic Dawn Center (DAWN), Denmark
2) Niels Bohr Institute, Denmark
3) GSI Helmholtzzentrum für Schwerionenforschung, Germany
4) Astrophysical Big Bang Laboratory, Japan
5) Department of Physics & Astronomy, University of Turku, Finland
6) School of Physics and Astronomy, Tel-Aviv University, Israel
7) Astrophysics Research Centre, Queen's University Belfast, UK

1

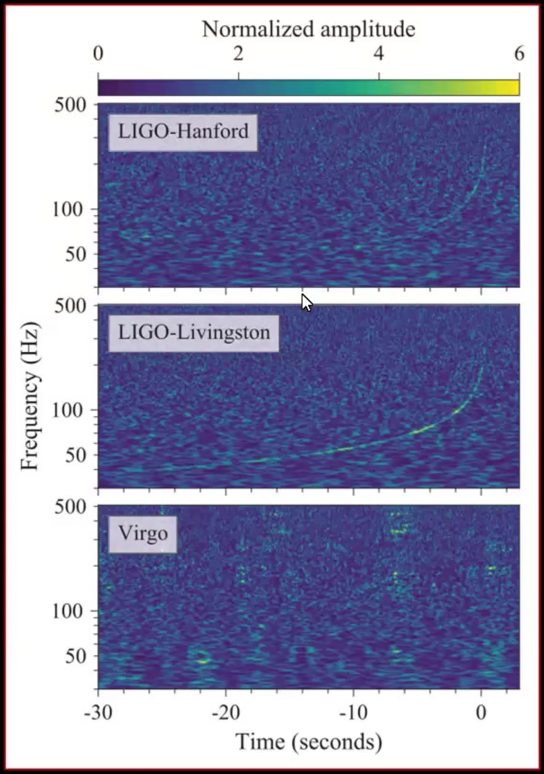
Normalized amplitude
0
2
4
6
500
LIGO-Hanford
100
50
500
LIGO-Livingston
Frequency (Hz)
100
50
500
Virgo
100
50
-30
-20
-10
0
Time (seconds)

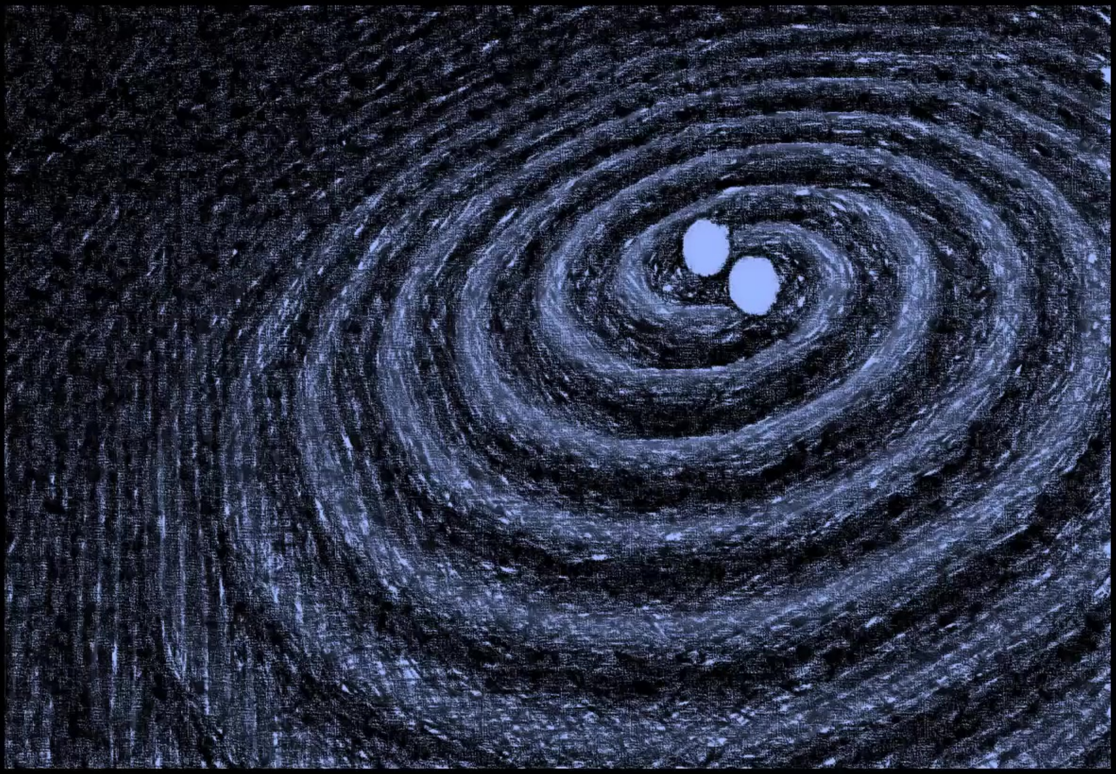

2

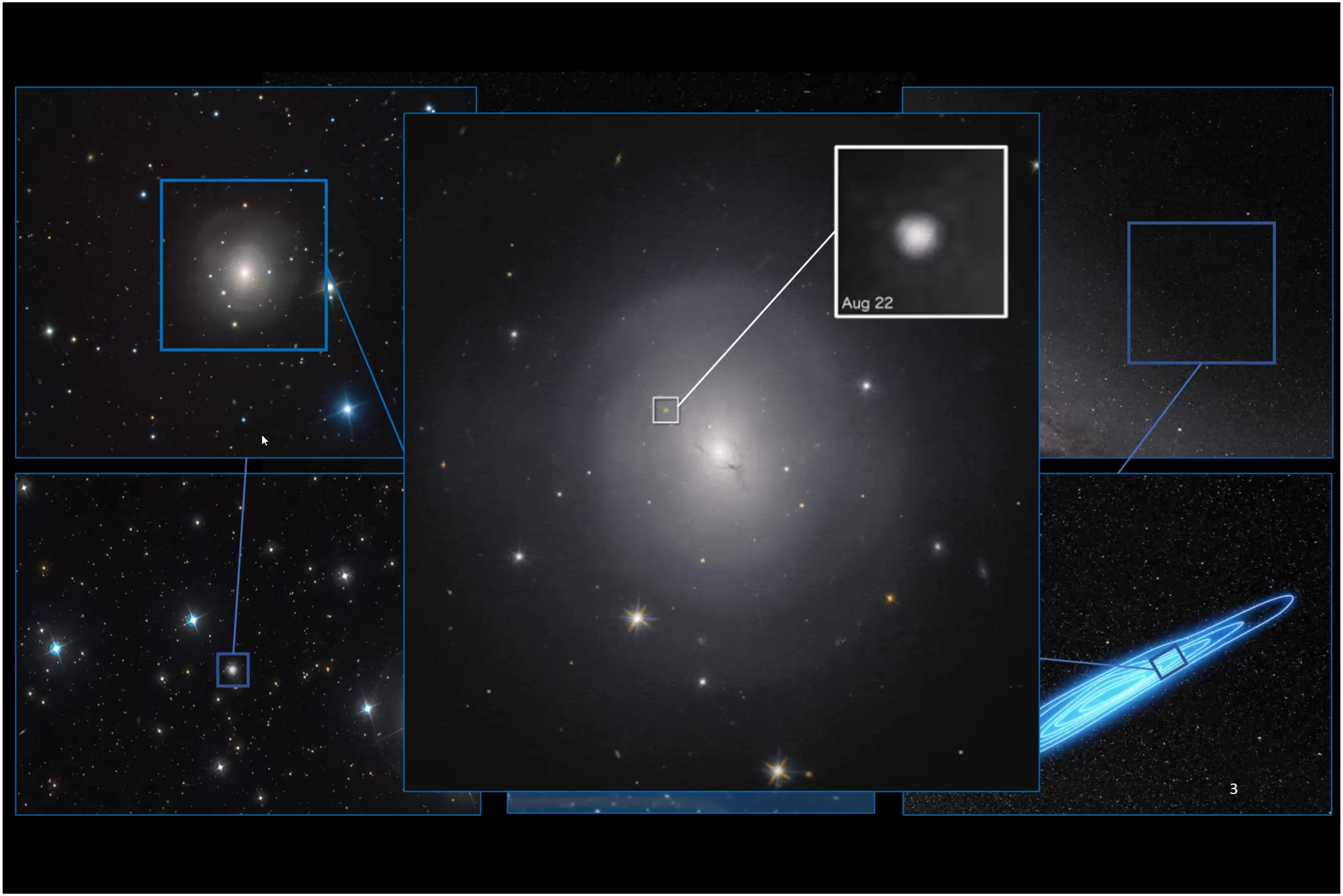
Aug 22
3

The Geometry of Expansion

Hanauske 2019

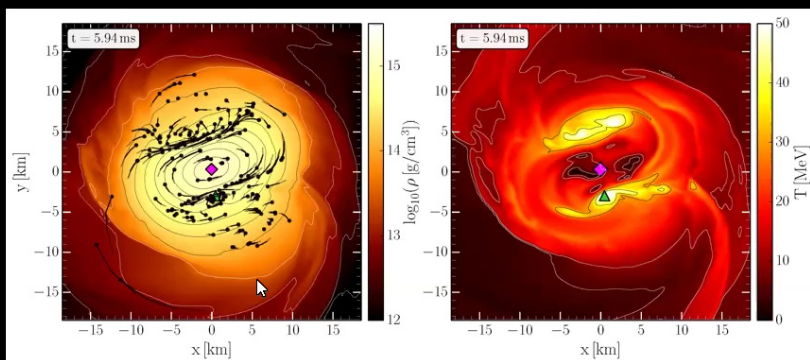

Just 2015

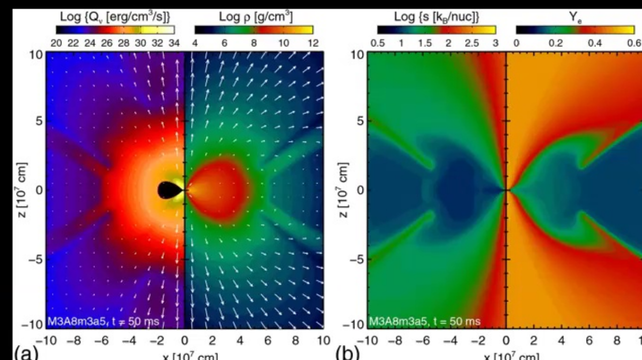

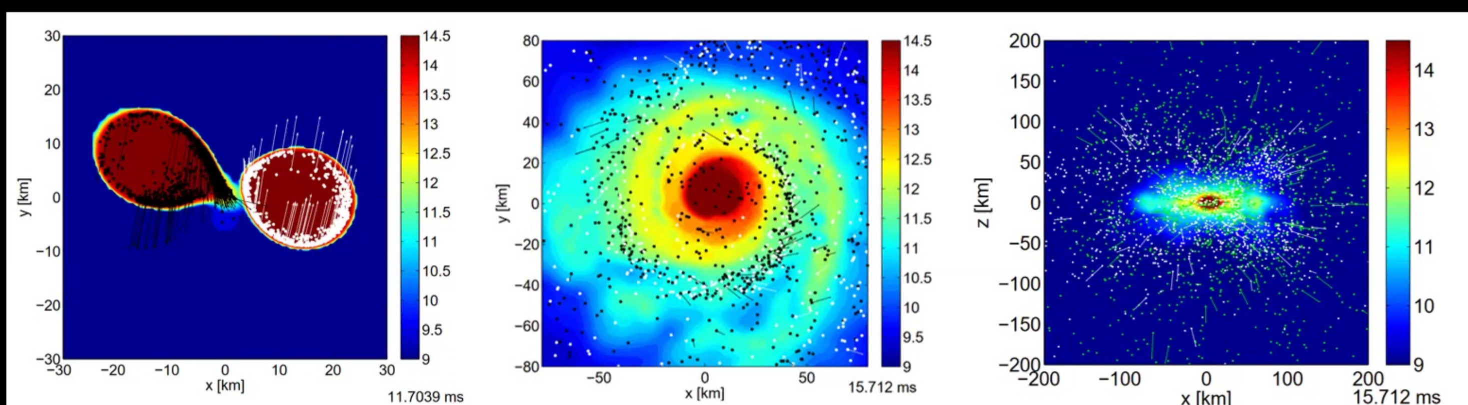

Bauswein 2013

4

Two complementary points of view;

1) The extreme physics of the merger

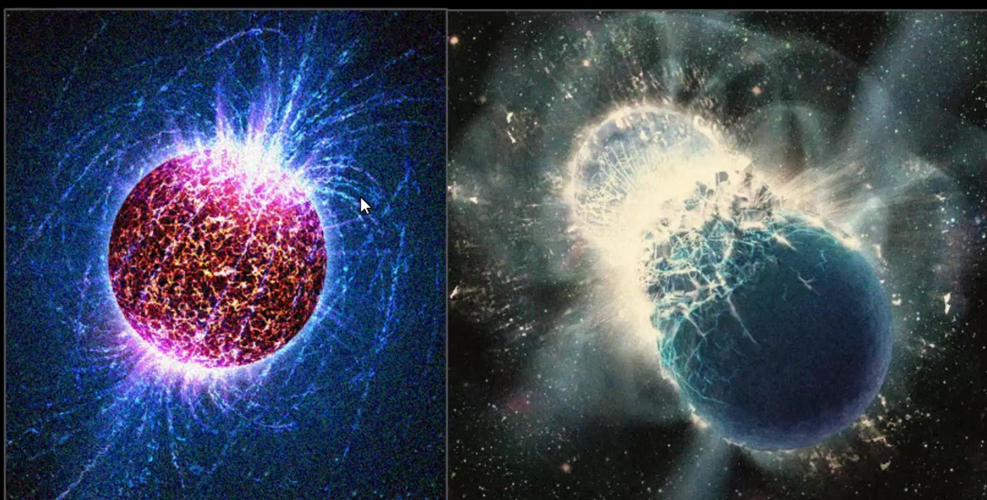

2) The Synthesis of the Heaviest Elements

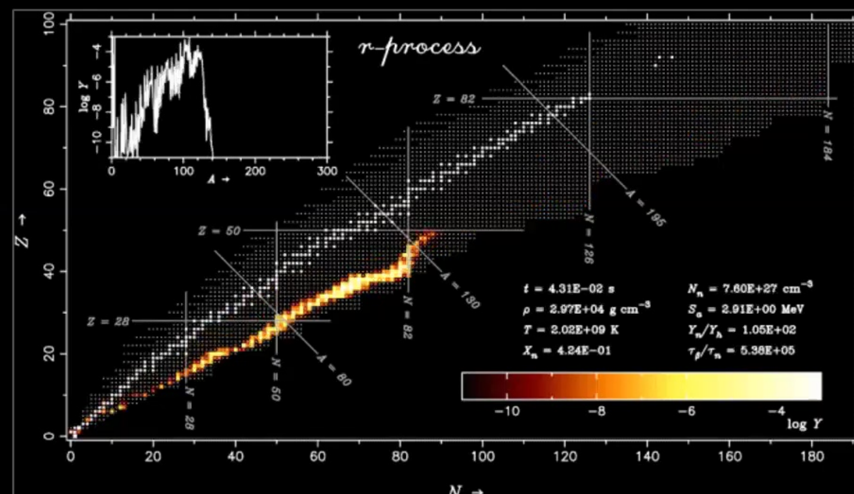

5

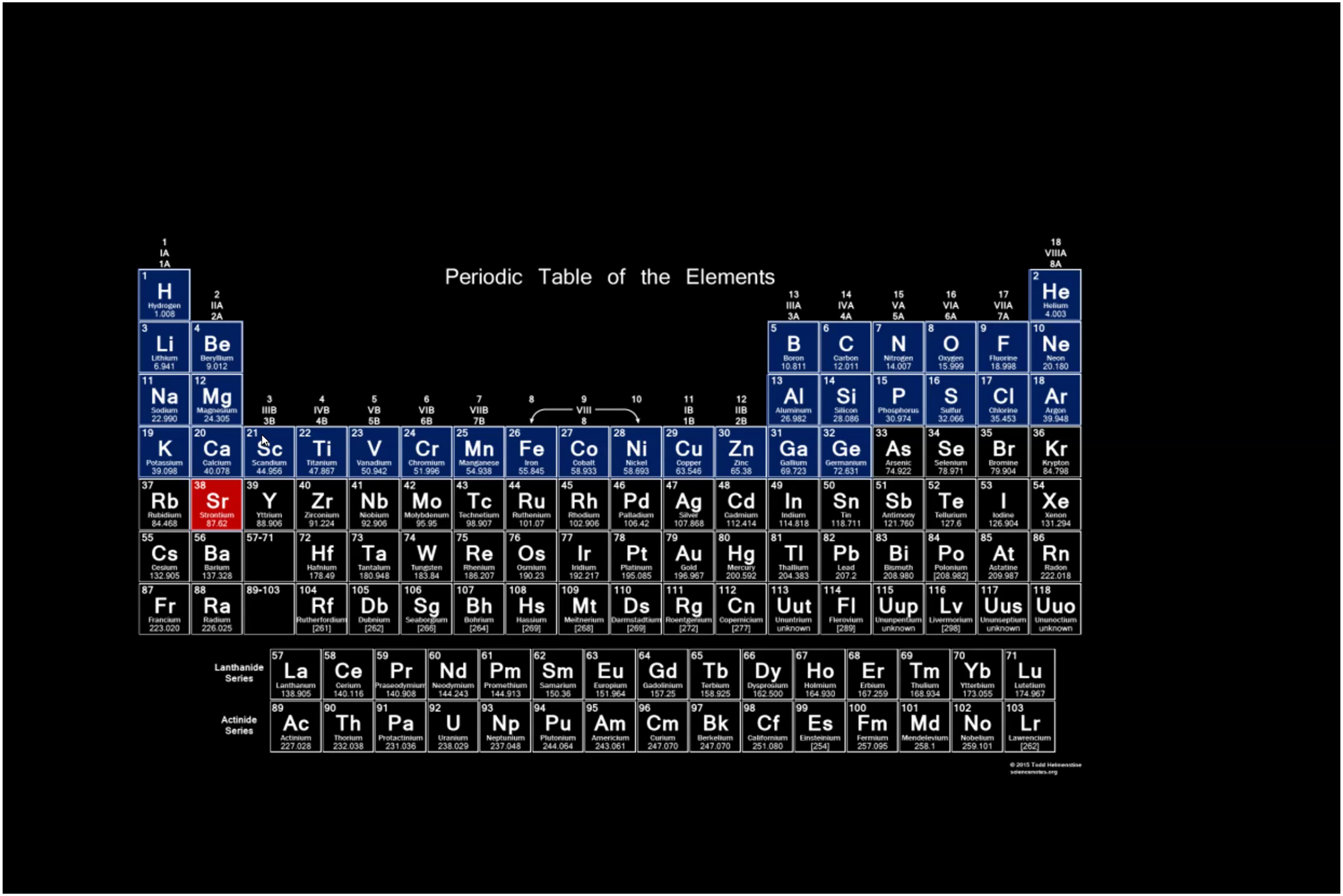
Periodic Table of the Elements
1 IA 1A
2 IIA 2A
3 IIIB 3B
4 IVB 4B
5 VB 5B
6 VIB 6B
7 VIIB 7B
8 VIII 8 9 10
11 IB 1B
12 IIB 2B
13 IIIA 3A
14 IVA 4A
15 VA 5A
16 VIA 6A
17 VIIA 7A
18 VIIIA 8A
1 H Hydrogen 1.008
2 He Helium 4.003
3 Li Lithium 6.941
4 Be Beryllium 9.012
5 B Boron 10.811
6 C Carbon 12.011
7 N Nitrogen 14.007
8 O Oxygen 15.999
9 F Fluorine 18.998
10 Ne Neon 20.180
11 Na Sodium 22.990
12 Mg Magnesium 24.305
13 Al Aluminum 26.982
14 Si Silicon 28.086
15 P Phosphorus 30.974
16 S Sulfur 32.066
17 Cl Chlorine 35.453
18 Ar Argon 39.948
19 K Potassium 39.098
20 Ca Calcium 40.078
21 Sc Scandium 44.956
22 Ti Titanium 47.867
23 V Vanadium 50.942
24 Cr Chromium 51.996
25 Mn Manganese 54.938
26 Fe Iron 55.845
27 Co Cobalt 58.933
28 Ni Nickel 58.693
29 Cu Copper 63.546
30 Zn Zinc 65.38
31 Ga Gallium 69.723
32 Ge Germanium 72.631
33 As Arsenic 74.922
34 Se Selenium 78.971
35 Br Bromine 79.904
36 Kr Krypton 84.798
37 Rb Rubidium 84.468
38 Sr Strontium 87.62
39 Y Yttrium 88.906
40 Zr Zirconium 91.224
41 Nb Niobium 92.906
42 Mo Molybdenum 95.95
43 Tc Technetium 98.907
44 Ru Ruthenium 101.07
45 Rh Rhodium 102.906
46 Pd Palladium 106.42
47 Ag Silver 107.868
48 Cd Cadmium 112.414
49 In Indium 114.818
50 Sn Tin 118.711
51 Sb Antimony 121.760
52 Te Tellurium 127.6
53 I Iodine 126.904
54 Xe Xenon 131.294
55 Cs Cesium 132.905
56 Ba Barium 137.328
57-71
72 Hf Hafnium 178.49
73 Ta Tantalum 180.948
74 W Tungsten 183.84
75 Re Rhenium 186.207
76 Os Osmium 190.23
77 Ir Iridium 192.217
78 Pt Platinum 195.085
79 Au Gold 196.967
80 Hg Mercury 200.592
81 Tl Thallium 204.383
82 Pb Lead 207.2
83 Bi Bismuth 208.980
84 Po Polonium [208.982]
85 At Astatine 209.987
86 Rn Radon 222.018
87 Fr Francium 223.020
88 Ra Radium 226.025
89-103
104 Rf Rutherfordium [261]
105 Db Dubnium [262]
106 Sg Seaborgium [266]
107 Bh Bohrium [264]
108 Hs Hassium [269]
109 Mt Meitnerium [268]
110 Ds Darmstadtium [269]
111 Rg Roentgenium [272]
112 Cn Copernicium [277]
113 Uut Ununtrium unknown
114 Fl Flerovium [289]
115 Uup Ununpentium unknown
116 Lv Livermorium [298]
117 Uus Ununseptium unknown
118 Uuo Ununoctium unknown
Lanthanide Series
57 La Lanthanum 138.905
58 Ce Cerium 140.116
59 Pr Praseodymium 140.908
60 Nd Neodymium 144.243
61 Pm Promethium 144.913
62 Sm Samarium 150.36
63 Eu Europium 151.964
64 Gd Gadolinium 157.25
65 Tb Terbium 158.925
66 Dy Dysprosium 162.500
67 Ho Holmium 164.930
68 Er Erbium 167.259
69 Tm Thulium 168.934
70 Yb Ytterbium 173.055
71 Lu Lutetium 174.967
Actinide Series
89 Ac Actinium 227.028
90 Th Thorium 232.038
91 Pa Protactinium 231.036
92 U Uranium 238.029
93 Np Neptunium 237.048
94 Pu Plutonium 244.064
95 Am Americium 243.061
96 Cm Curium 247.070
97 Bk Berkelium 247.070
98 Cf Californium 251.080
99 Es Einsteinium [254]
100 Fm Fermium 257.095
101 Md Mendelevium 258.1
102 No Nobelium 259.101
103 Lr Lawrencium [262]

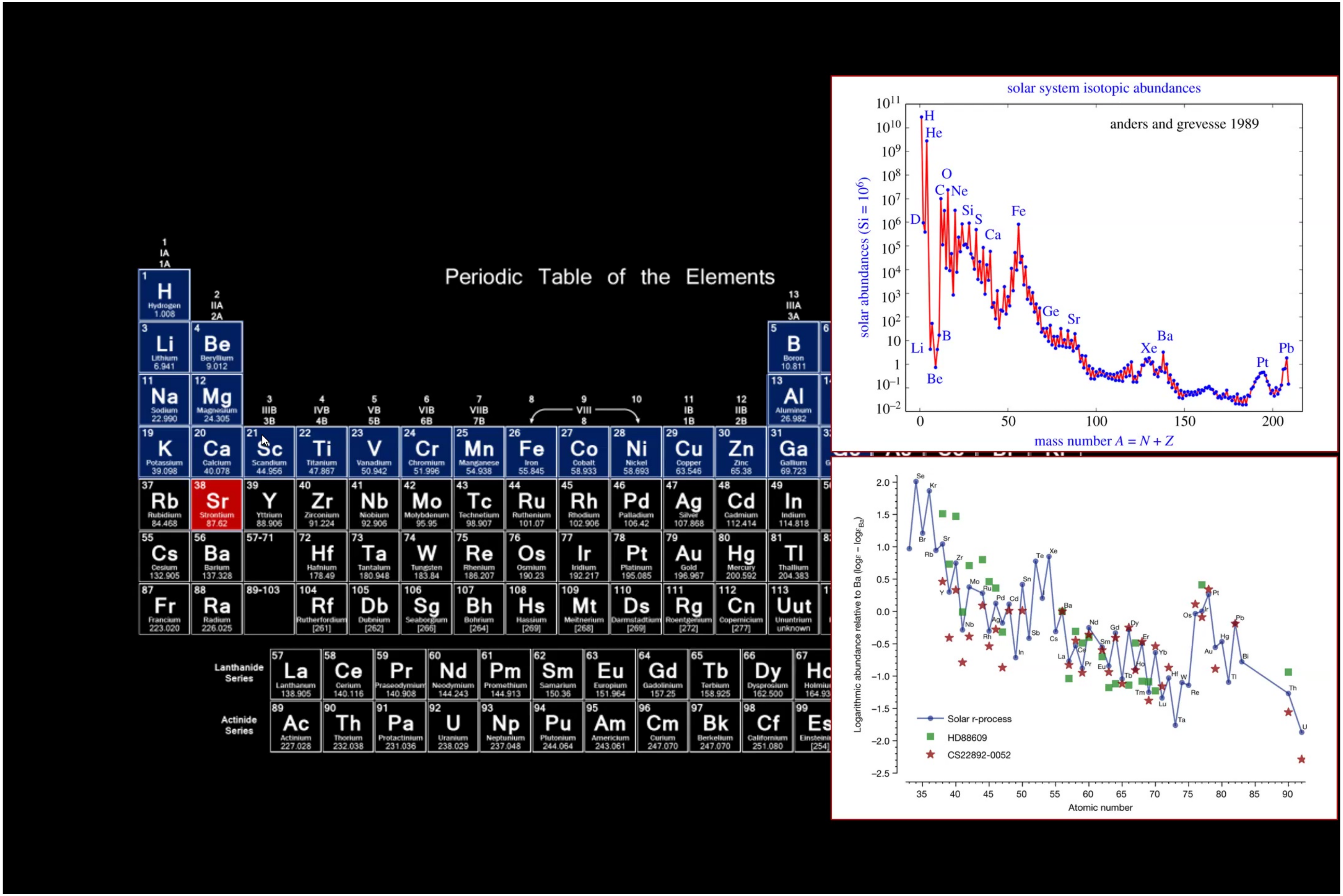
Periodic Table of the Elements
solar system isotopic abundances
anders and grevesse 1989
solar abundances (Si = 10^6)
mass number A = N + Z
Logarithmic abundance relative to Ba
Atomic number
Solar r-process
HD88609
CS22892-0052

Two complementary points of view;

1) The extreme physics of the merger

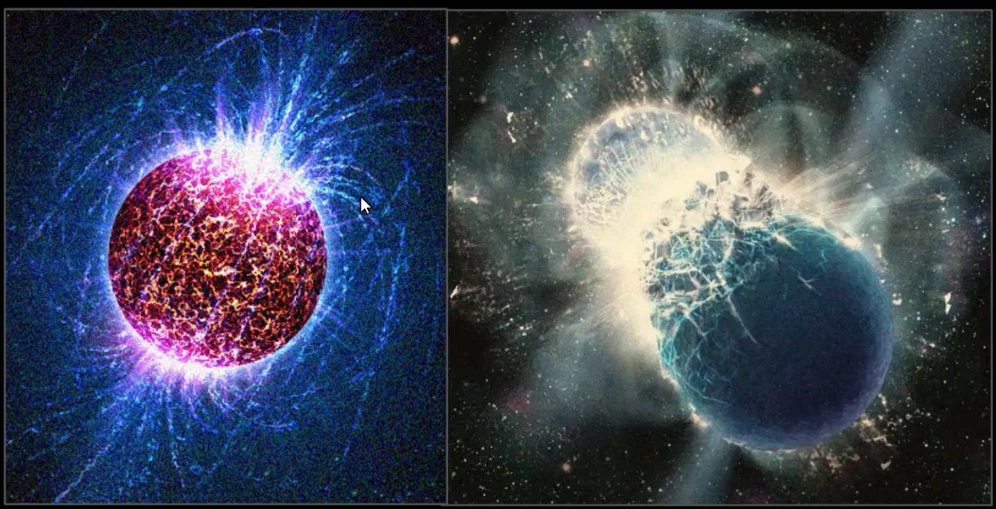

2) The Synthesis of the Heaviest Elements

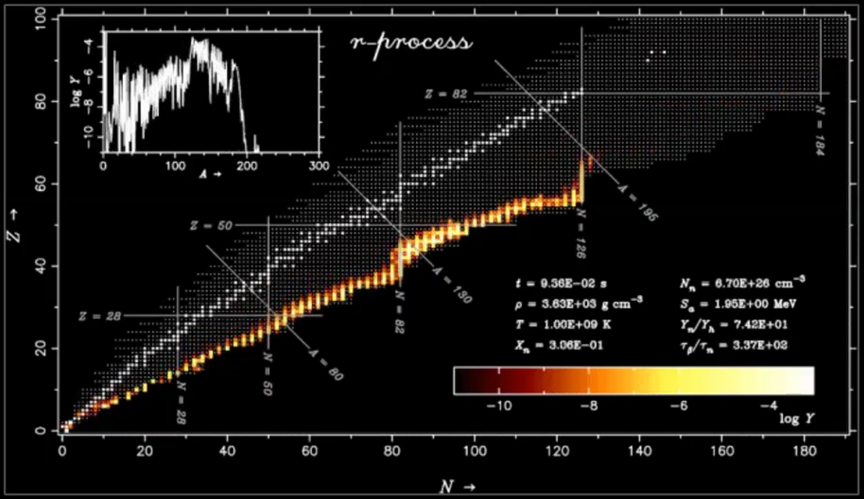

8

The Geometry of Expansion

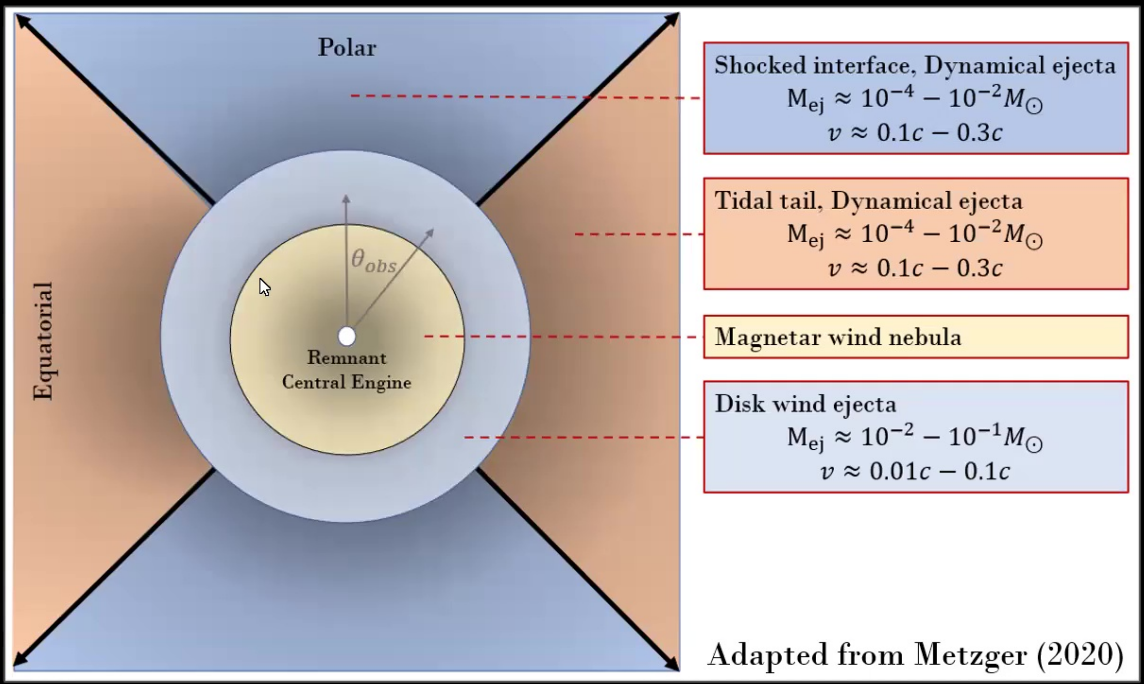

Series of different mass ejection channels with varying geometry.

Prior Geometrical Constraints

Covino et al. (2017): *"The low degree of polarization is consistent with intrinsically unpolarized emission scattered by Galactic dust, suggesting a symmetric geometry of the emitting region and low inclination of the merger system."*

For a detailed analysis of the linear polarization expected from kilonovae with 3D Monte Carlo radiative transfer simulations - see Bulla et al (2019): *"The origin of polarization in kilonovae and the case of the gravitational-wave counterpart AT 2017gfo"*

Covino et al. (2017):

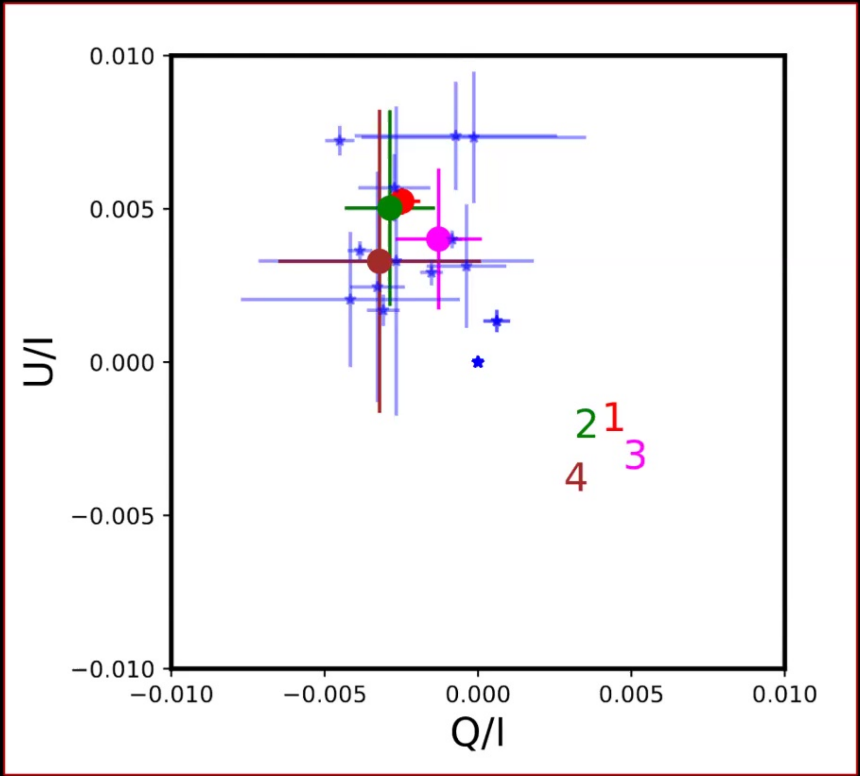

10

Kilonova AT2017gfo

Villar (2017)

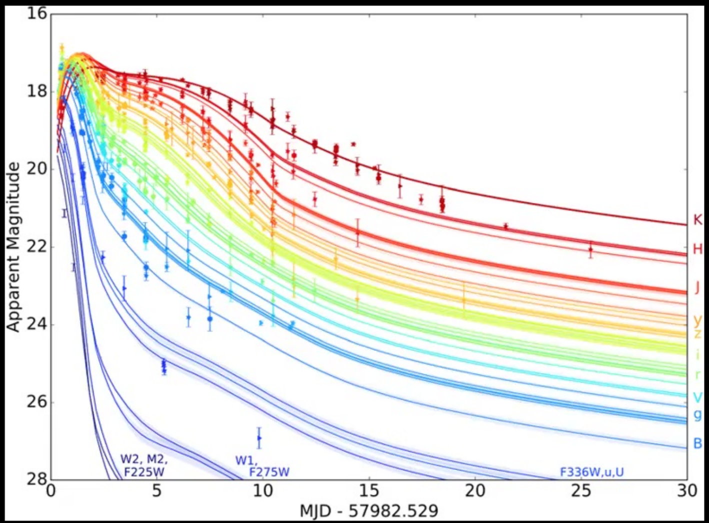

VLT/X-Shooter Spectra, Data from Pian et al. (2017)

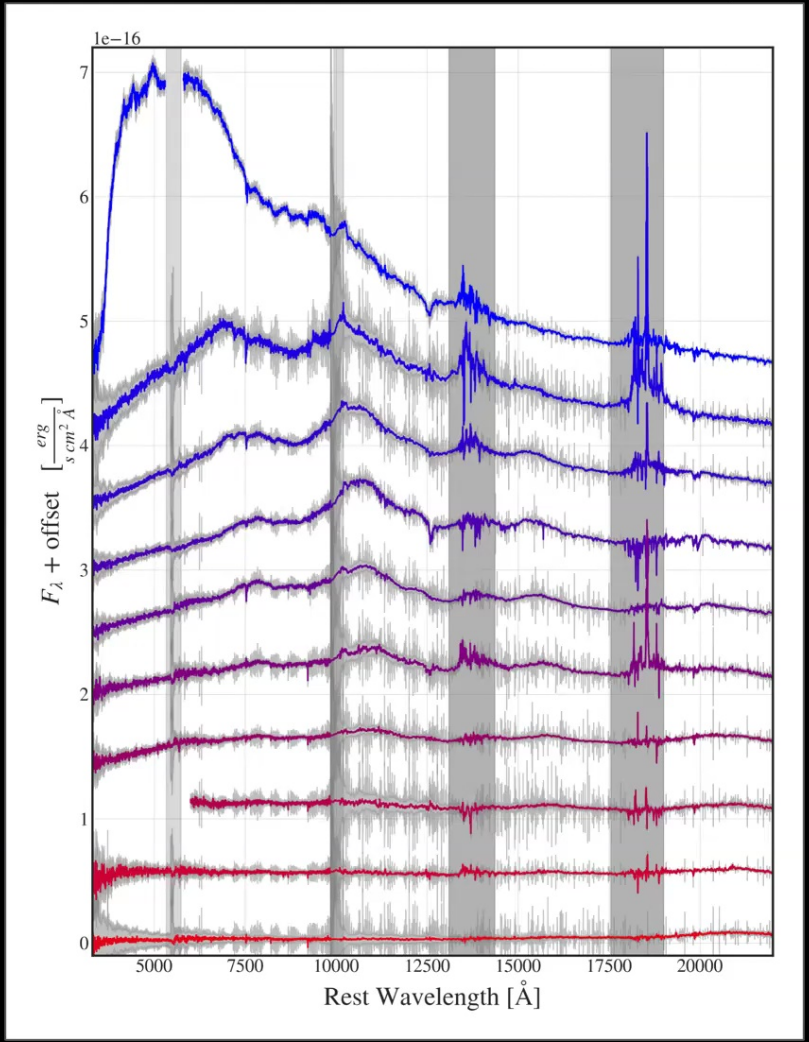

AT2017gfo

Continuum well-modelled by a blackbody*:

$$B_\lambda(T_{\mathrm{eff}}) = \frac{2\,h\,c^2}{\lambda^5}\frac{1}{\left(e^{\frac{hc}{\lambda k_B T_{eff}}} - 1\right)}$$

*A blackbody is empirically well-validated in early epochs. But radiative transfer modelling has a hard time reproducing the observed spectrum [for a derivation of the blackbody formulation, see Sneppen (2023), in prep]

Watson et al. (2019)

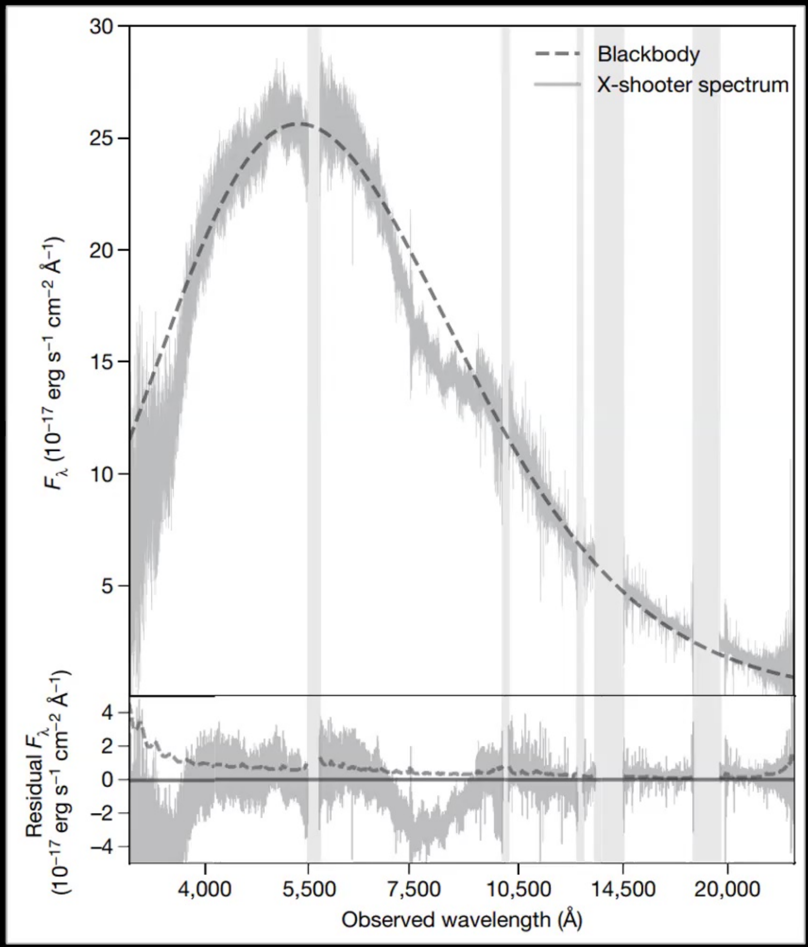

12

AT2017gfo

Continuum well-modelled by a blackbody:

$$B_\lambda(T_{\rm eff}) = \frac{2\,h\,c^2}{\lambda^5}\frac{1}{\left(e^{\frac{hc}{\lambda k_B T_{eff}}} - 1\right)}$$

with an absorption/emission component of Sr^+

For deliberation on the identification of Sr, see for instance:

- **Watson et al (2019),**
- **Domoto et al. (2021),**
- **Gillanders et al. (2022),**
- **Vieira et al. (2023)**

X-shooter spectrum epoch 1+2

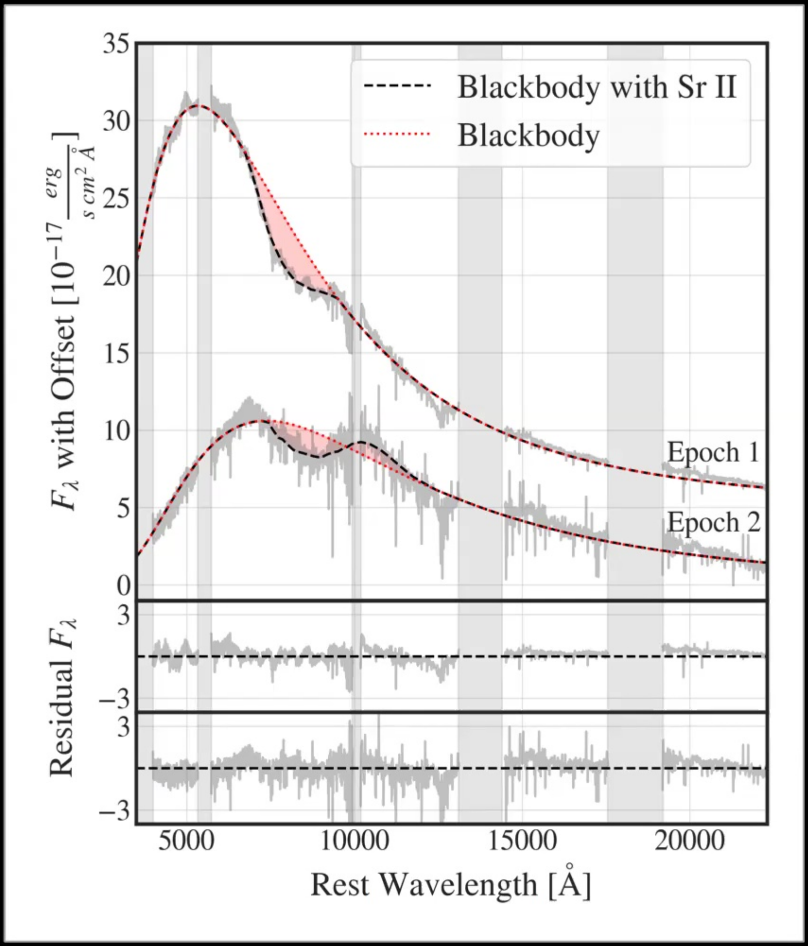

The information *hiding* in the line

illustration from Dan Kasen

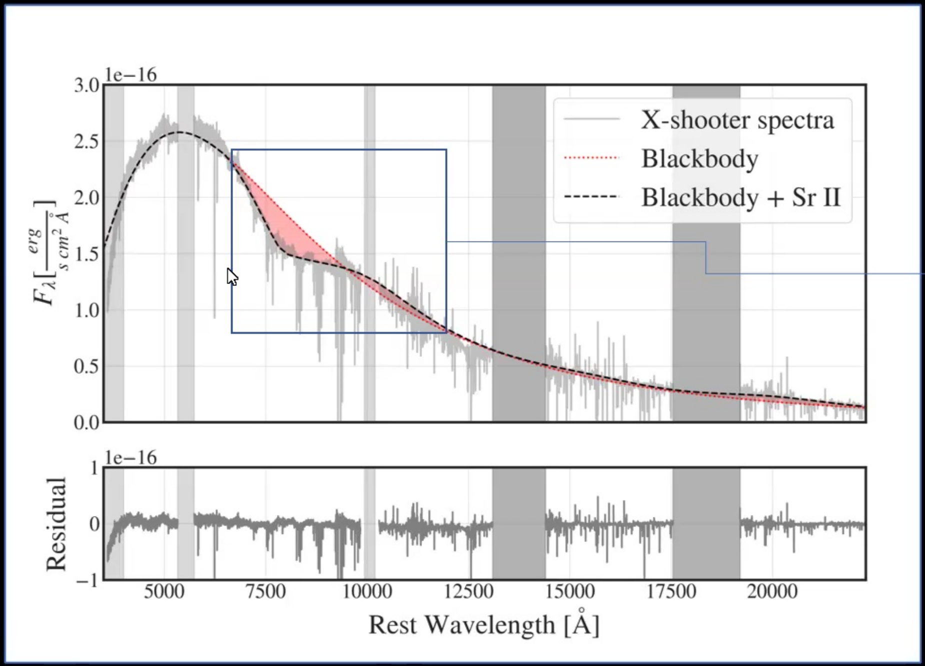

X-shooter spectrum epoch 1

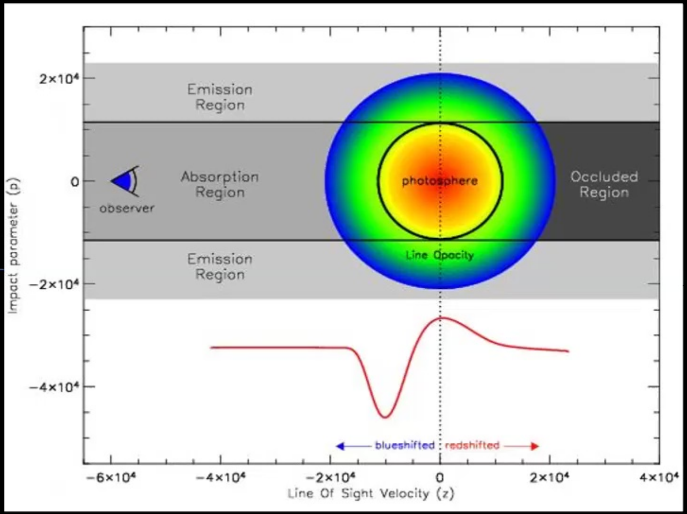

Parameterization of P Cygni profile in the Elementary Supernova from https://github.com/unoebauer/public-astro-tools

The Expanding Photosphere Method

Introduced for SNe in Baade (1926) , Kirshner (1974)

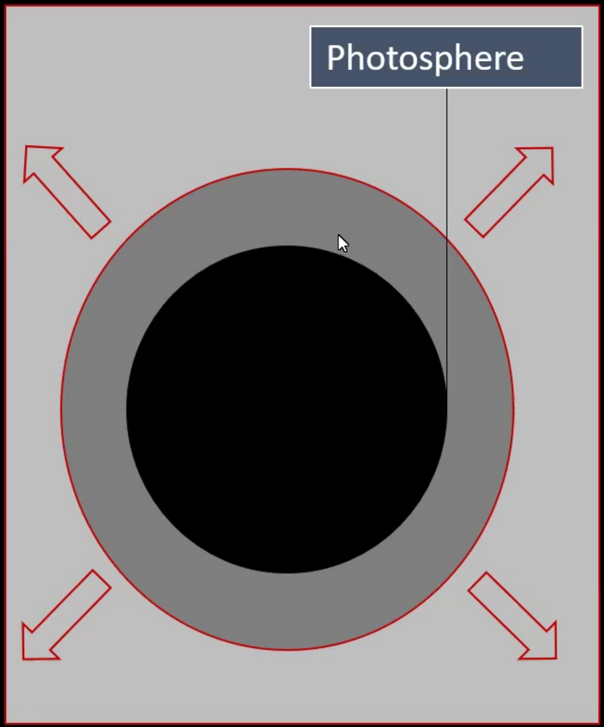

Assumptions:

1) Blackbody spectrum, $B_\lambda(T)$

2) Homologues expansion

$$R_{ph} = v_{exp} \cdot (t - t_e)$$

3) Optically thick

4) Spherical Symmetry

$$\rightarrow L_\lambda = 4\pi R^2 \pi B_\lambda(T)$$

Yielding a distance:

$$D_L = R_{ph} \sqrt{\frac{\pi B_\lambda(T_{eff})}{F_\lambda f(\beta)}}$$

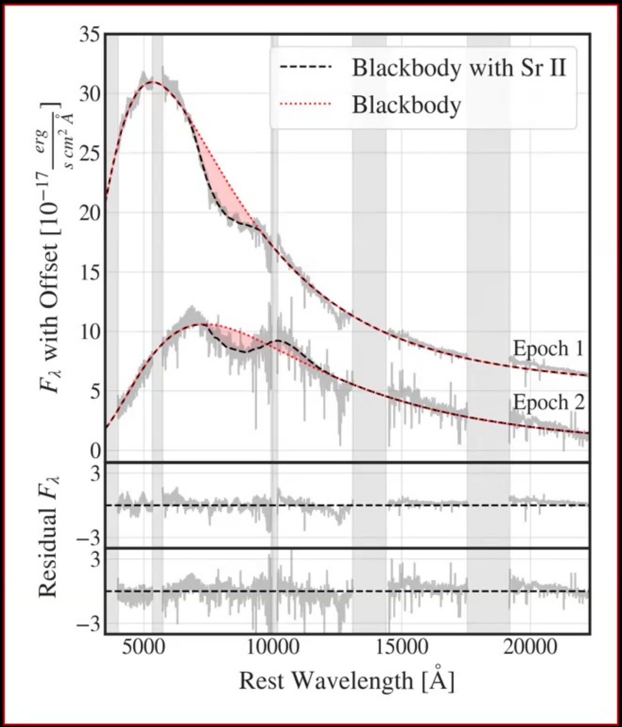

The Expanding Photosphere Method

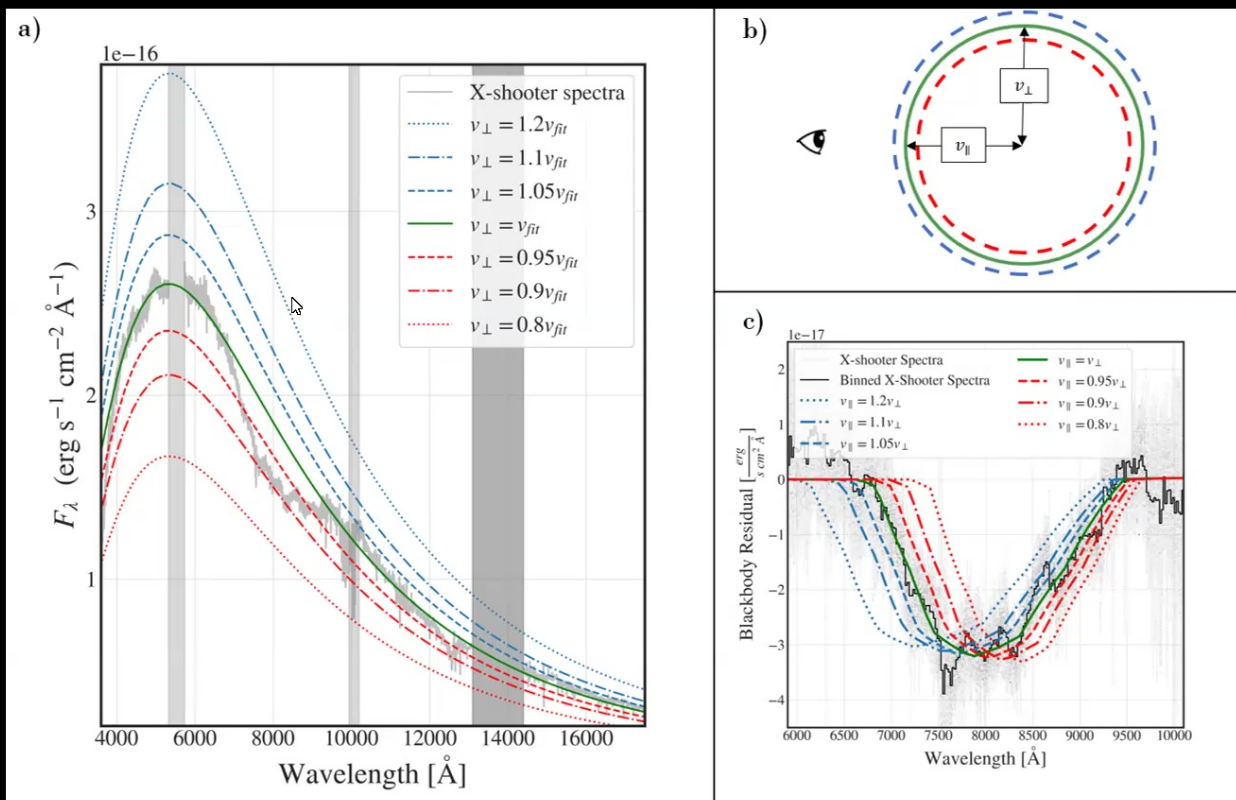

Sneppen, A., Watson, D. et al (2023)

$v_\perp$: The cross-sectional velocity (inferred from the continuum luminosity)

$v_\parallel$: The velocity along the line-of-sight (inferred from the 1 μm P Cygni)

16

The Expanding Photosphere Method

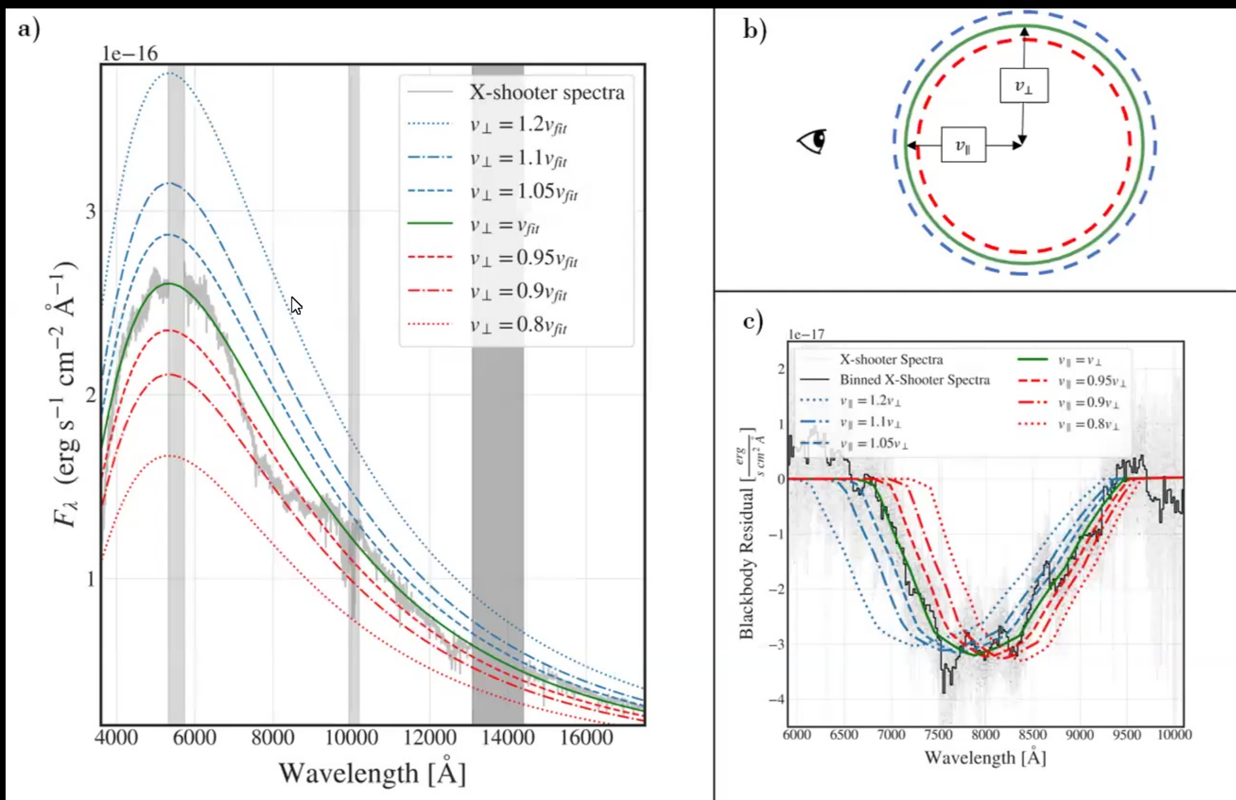

Sneppen, A., Watson, D. et al (2023)

$v_\perp$: The cross-sectional velocity (inferred from the continuum luminosity)

$v_\parallel$: The velocity along the line-of-sight (inferred from the 1 μm P Cygni)

$$\Upsilon = \frac{v_\parallel - v_\perp}{v_\parallel + v_\perp}$$

17

A Spherical Expansion - I

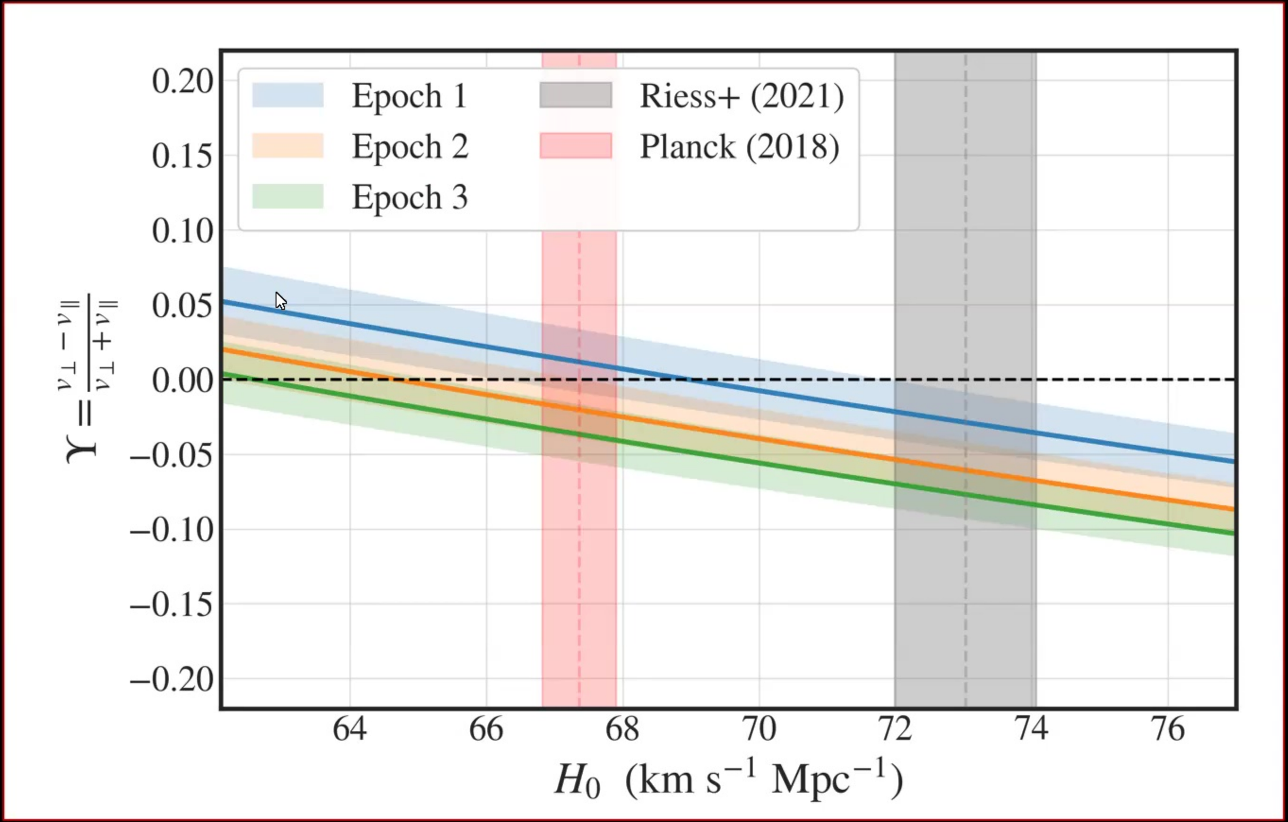

Sneppen, A.,Watson, D. et al (2023)

18

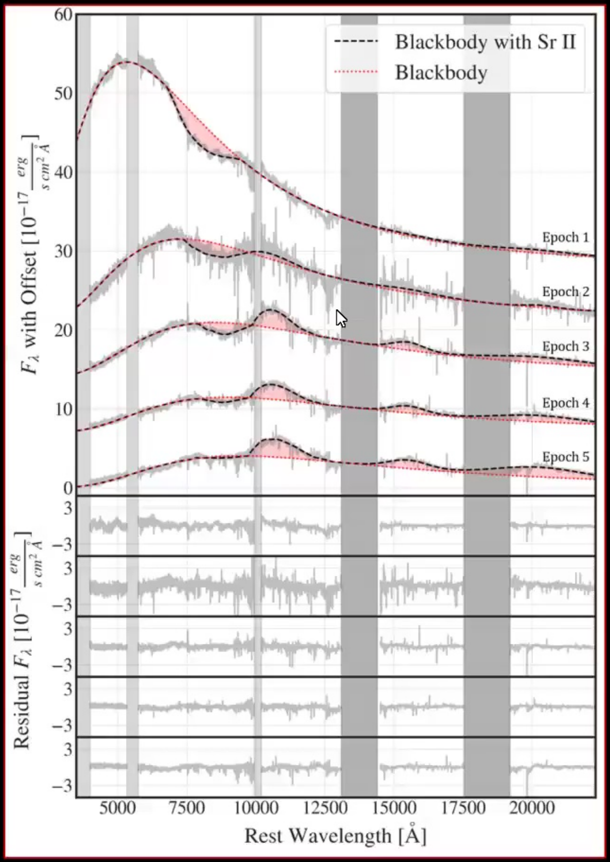
Blackbody with Sr II
Blackbody
Epoch 1
Epoch 2
Epoch 3
Epoch 4
Epoch 5
F_λ with Offset $[10^{-17} \frac{erg}{s\,cm^2\,Å}]$
Residual F_λ $[10^{-17} \frac{erg}{s\,cm^2\,Å}]$
Rest Wavelength [Å]
0
10
20
30
40
50
60
3
−3
5000
7500
10000
12500
15000
17500
20000

19

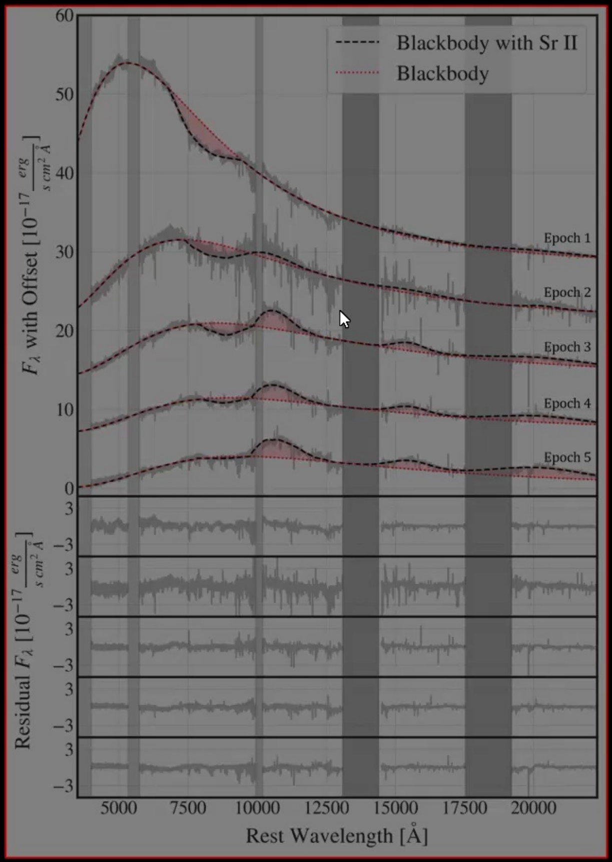
Blackbody with Sr II
Blackbody
Epoch 1
Epoch 2
Epoch 3
Epoch 4
Epoch 5
F_λ with Offset $[10^{-17} \frac{erg}{s\,cm^2\,Å}]$
Residual F_λ $[10^{-17} \frac{erg}{s\,cm^2\,Å}]$
Rest Wavelength [Å]

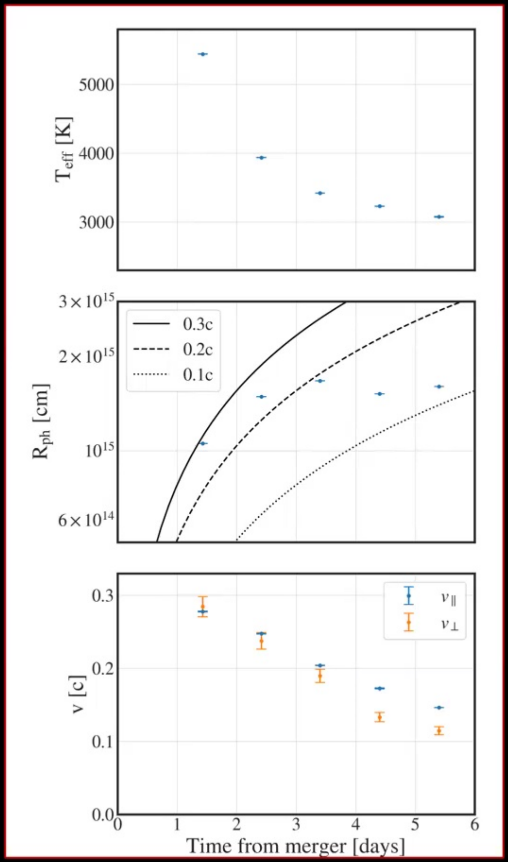
T_{eff} [K]
R_{ph} [cm]
0.3c
0.2c
0.1c
$v_\parallel$
$v_\perp$
v [c]
Time from merger [days]

20

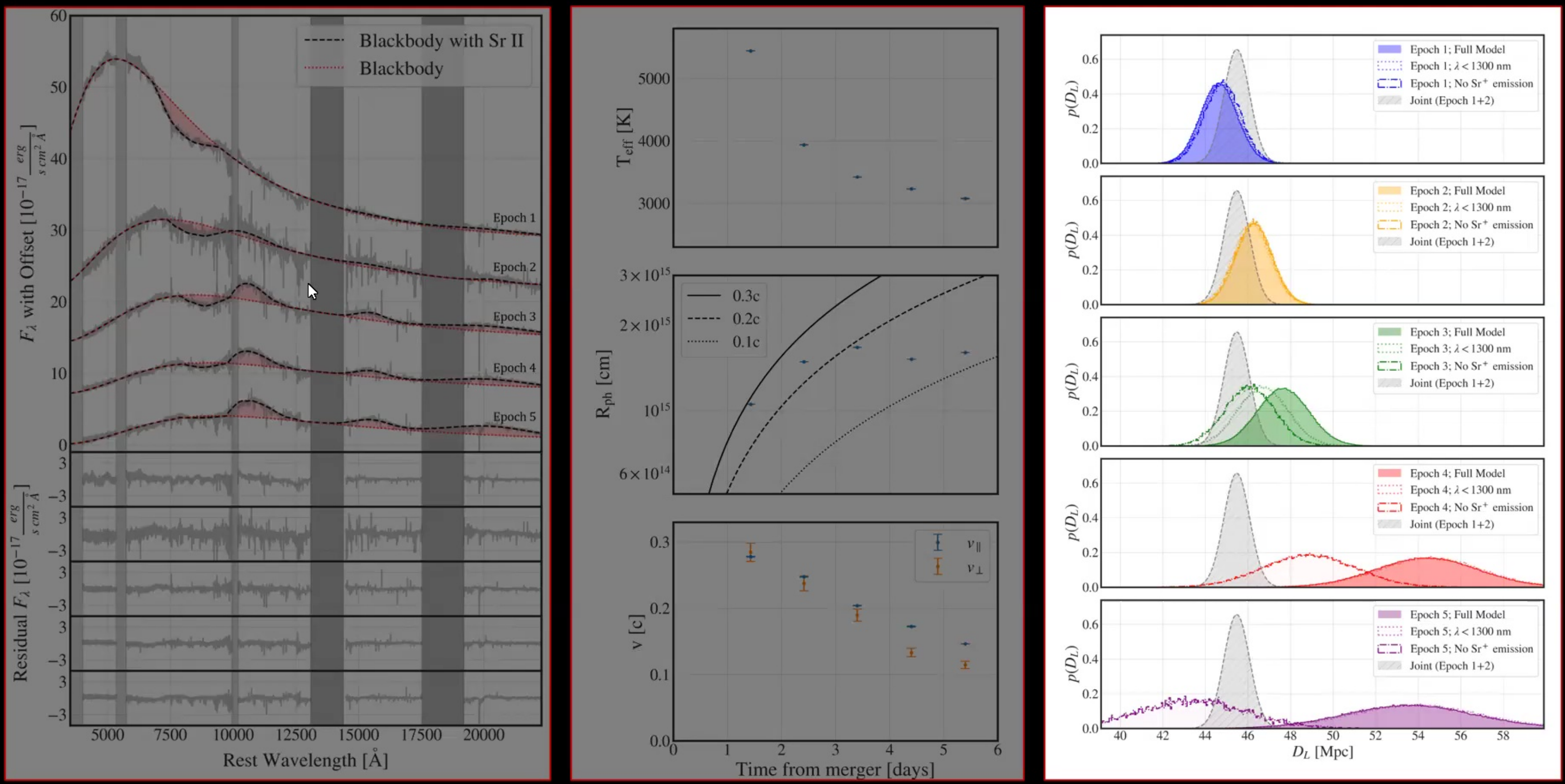

Blackbody with Sr II
Blackbody
Epoch 1
Epoch 2
Epoch 3
Epoch 4
Epoch 5
F_λ with Offset $[10^{-17} \frac{erg}{s\,cm^2\,Å}]$
Residual F_λ $[10^{-17} \frac{erg}{s\,cm^2\,Å}]$
Rest Wavelength [Å]
T_{eff} [K]
R_{ph} [cm]
0.3c
0.2c
0.1c
v [c]
$v_\parallel$
$v_\perp$
Time from merger [days]
Epoch 1; Full Model
Epoch 1; $\lambda < 1300$ nm
Epoch 1; No Sr^+ emission
Joint (Epoch 1+2)
Epoch 2; Full Model
Epoch 2; $\lambda < 1300$ nm
Epoch 2; No Sr^+ emission
Epoch 3; Full Model
Epoch 3; $\lambda < 1300$ nm
Epoch 3; No Sr^+ emission
Epoch 4; Full Model
Epoch 4; $\lambda < 1300$ nm
Epoch 4; No Sr^+ emission
Epoch 5; Full Model
Epoch 5; $\lambda < 1300$ nm
Epoch 5; No Sr^+ emission
$p(D_L)$
D_L [Mpc]

21

A Spherical Expansion - I

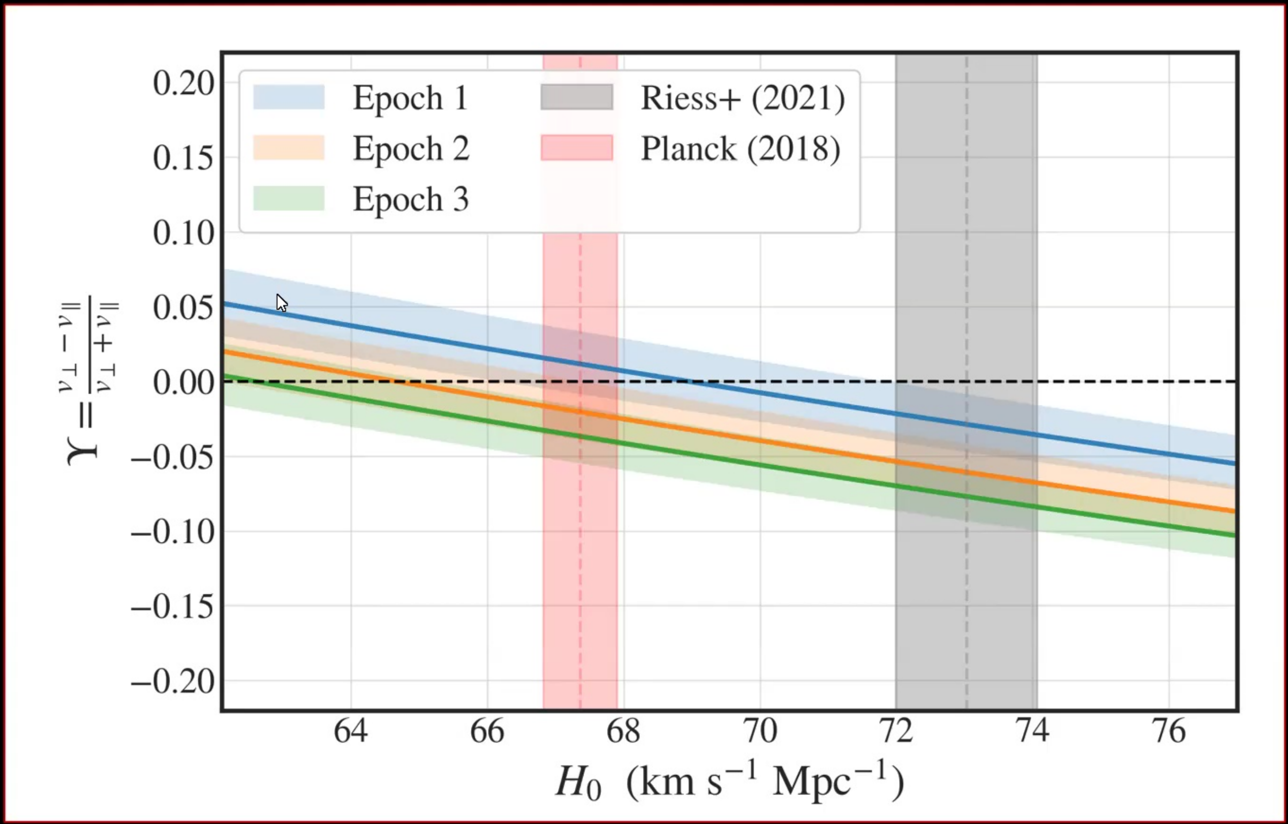

Sneppen, A.,Watson, D. et al (2023)

Kilonovae are optimal for EPM

1) GW yield tight constraints on timing (thus each epoch is statistically independent)

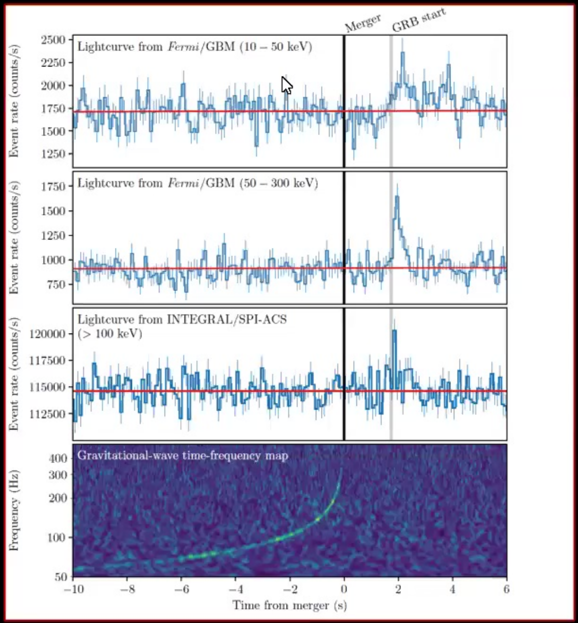

LIGO Collaboration (2017)

23

Kilonovae are optimal for EPM

1) GW yield tight constraints on timing (thus each epoch is statistically independent)
2) *The rapid follow-up allows a temporal examination of the evolving ejected material*

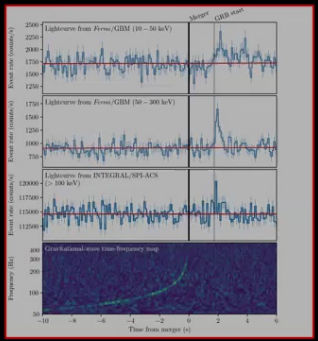

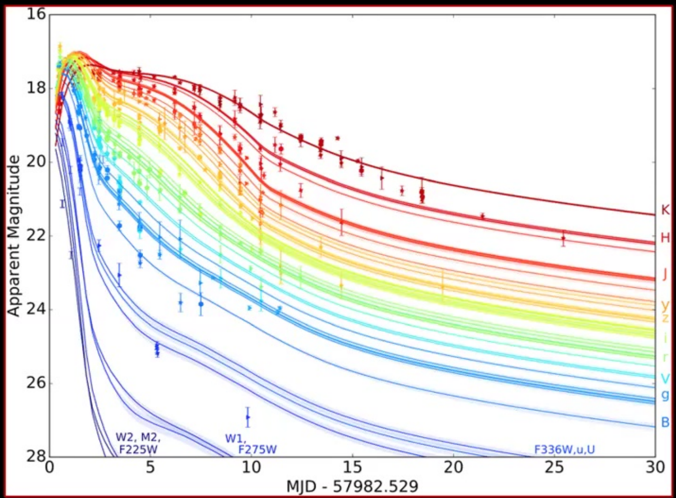

Villar et al (2017)

24

Kilonovae are optimal for EPM

1) GW yield tight constraints on timing (thus each epoch is statistically independent)
2) The rapid follow-up allows a temporal examination of the evolving ejected material
3) *The velocity of the ejected material is large allowing a detailed velocity stratification of the P Cygni profile.*

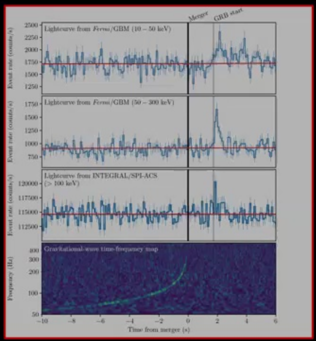

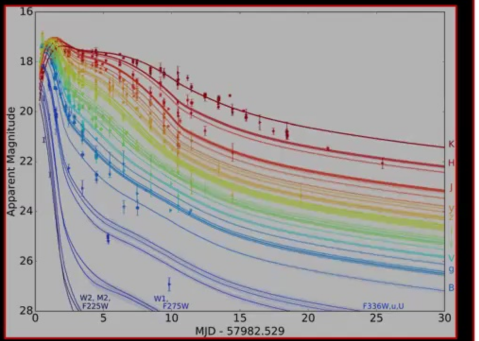

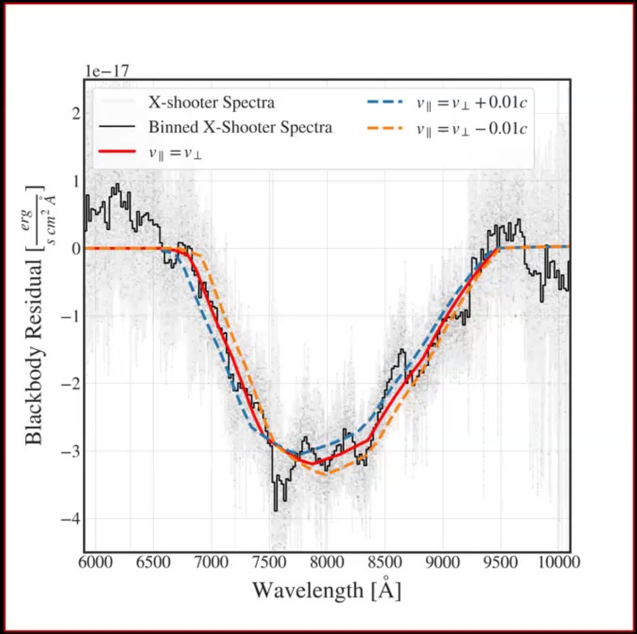

Kilonovae are optimal for EPM

1) GW yield tight constraints on timing (thus each epoch is statistically independent)
2) The rapid follow-up allows a temporal examination of the evolving ejected material
3) The velocity of the ejected material is large allowing a detailed velocity stratification of the P Cygni profile.
4) *Electron scattering is negligible. No requirement for large dilution factors.*

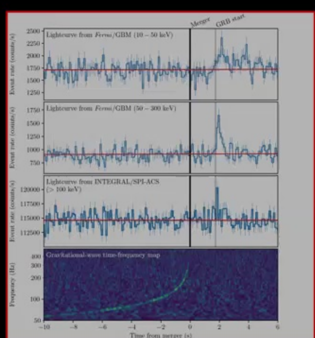

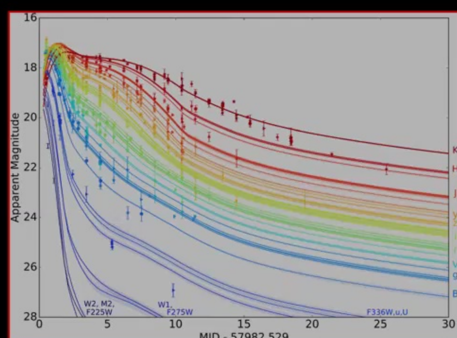

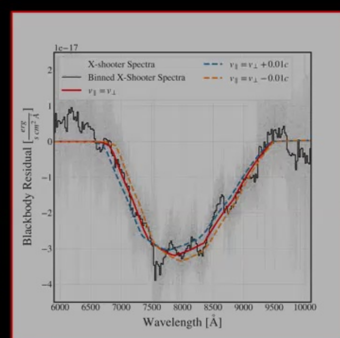

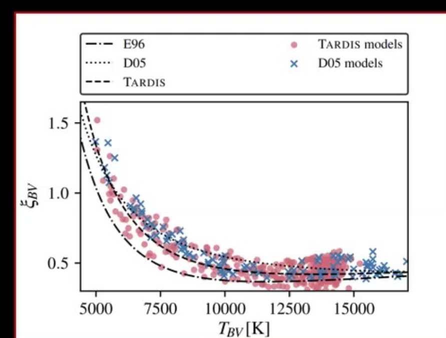

Vogl et al (2019)

Dilution factors Exemplified

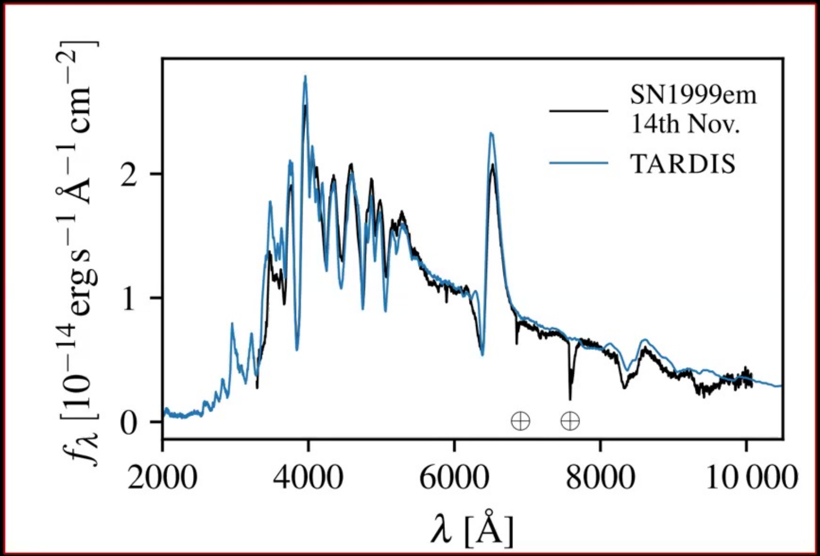

Vogl 2018; SN1999em

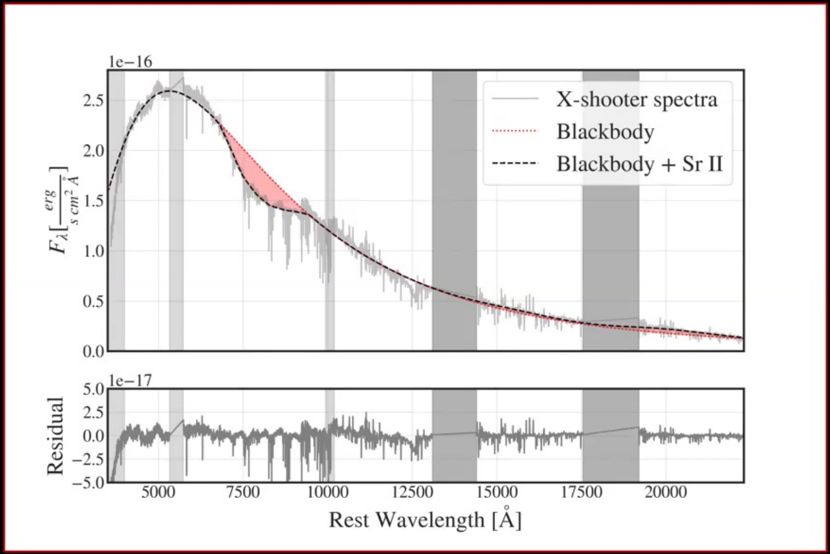

X-shooter spectrum AT2017gfo

27

Varying ellipticity

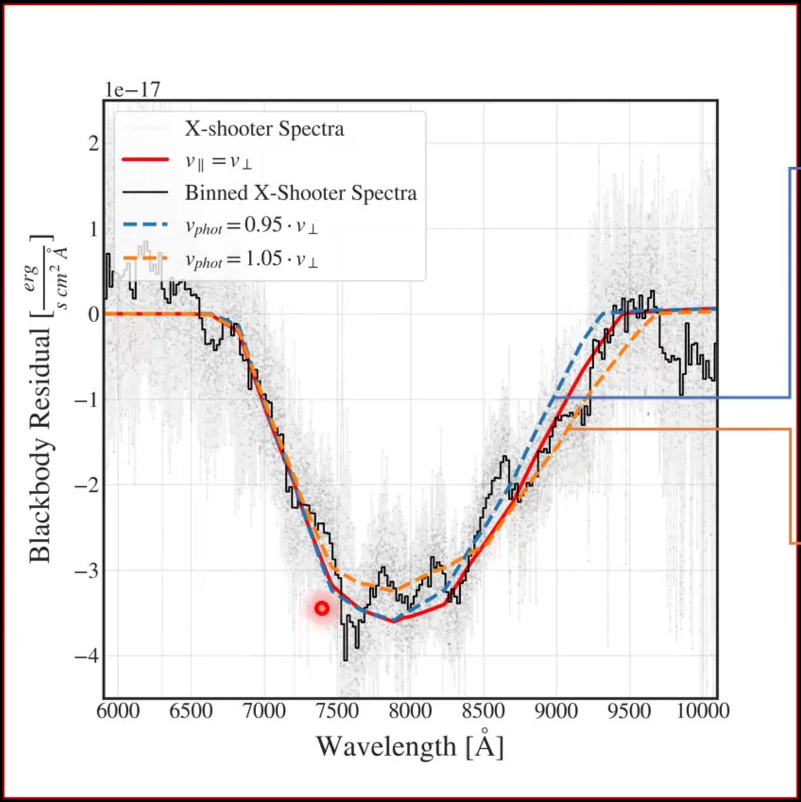

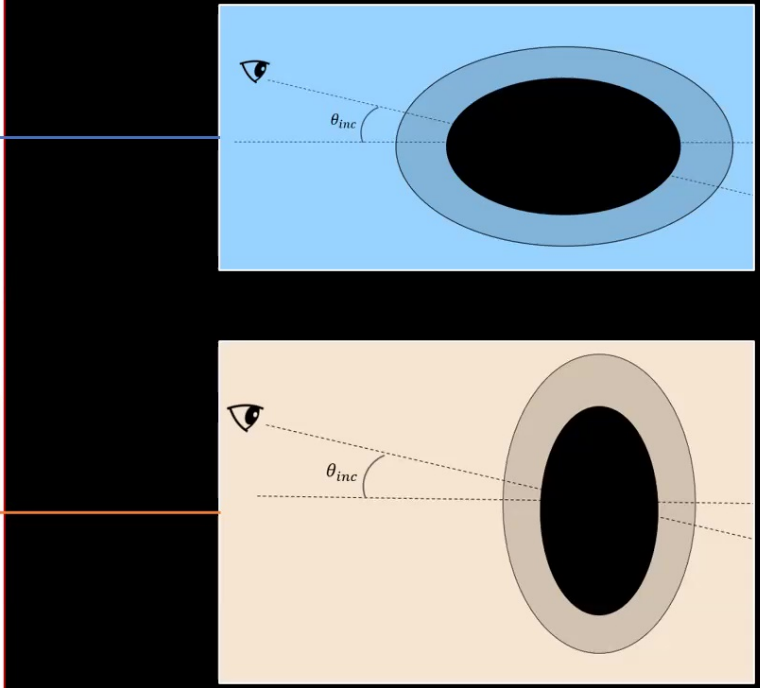

28

Fitting ellipsoidal photosphere

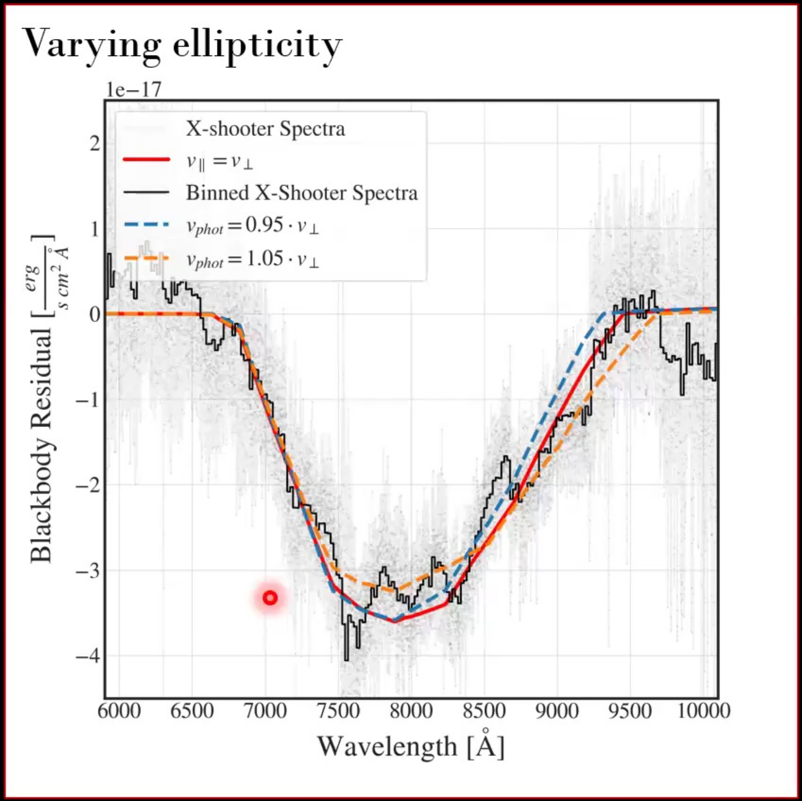

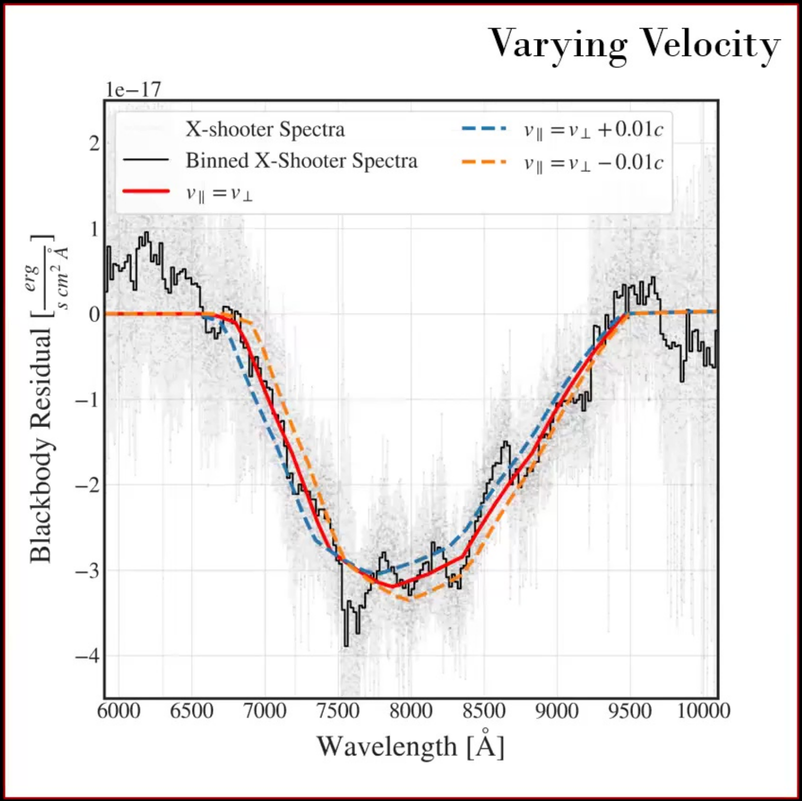

29

Degenerate?

Example Degenerate Landscape

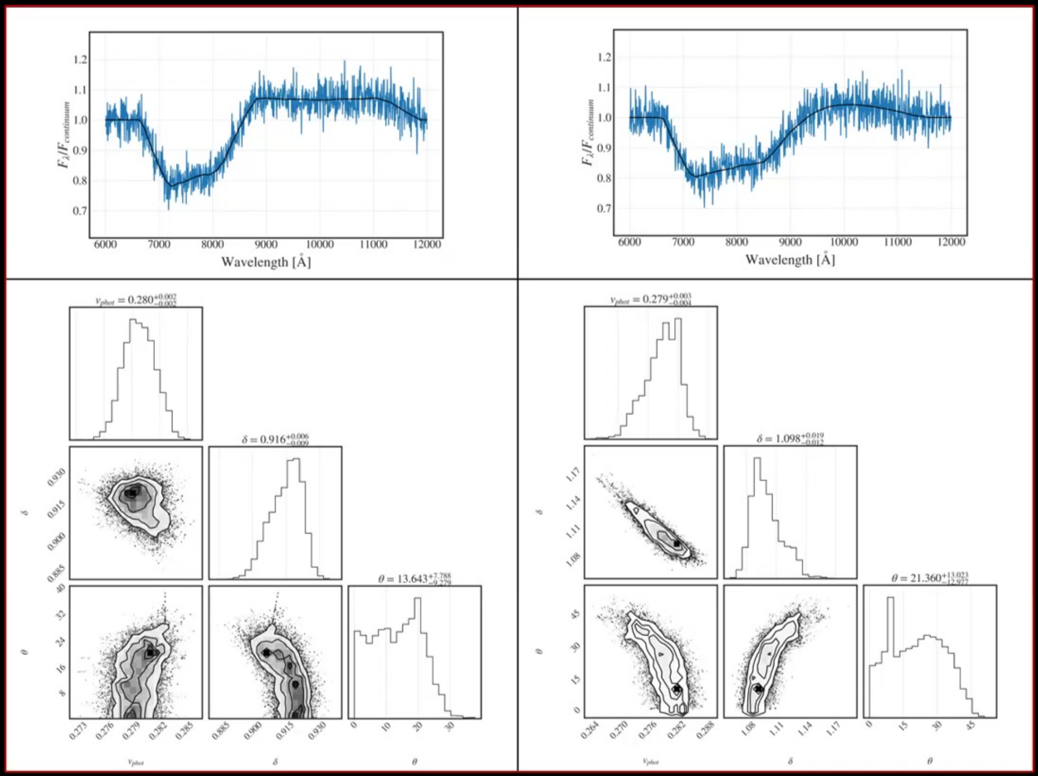

Höflich et al (1997)

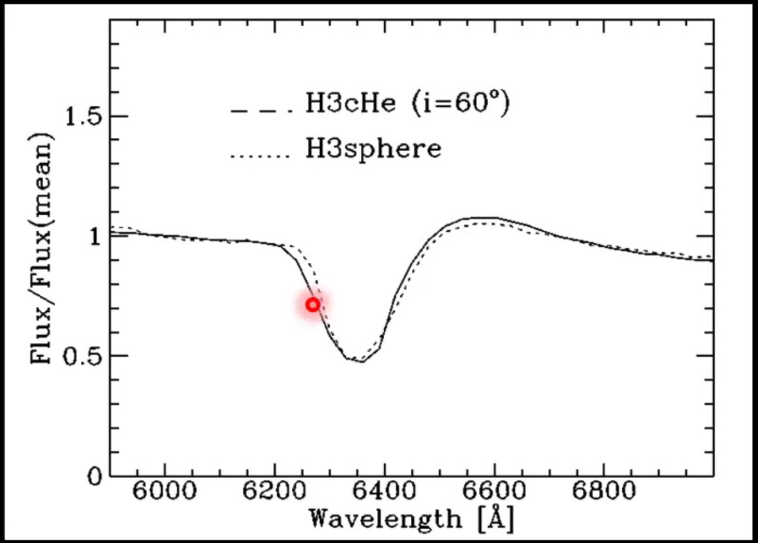

30

Degenerate, but inclination-angle is known

Example Degenerate Landscape

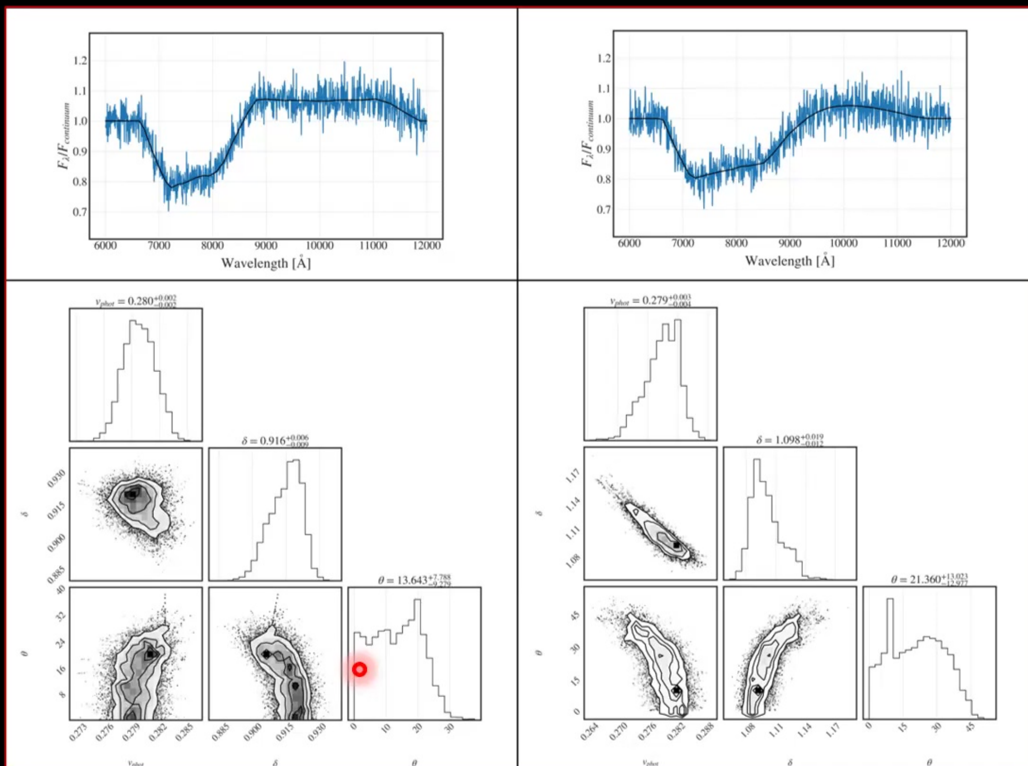

VLBI [Mooley et al (2017)]

+ Hubble Precision Astrometry [Mooley et al (2022)]

= breaks degeneracy with inclination-angle

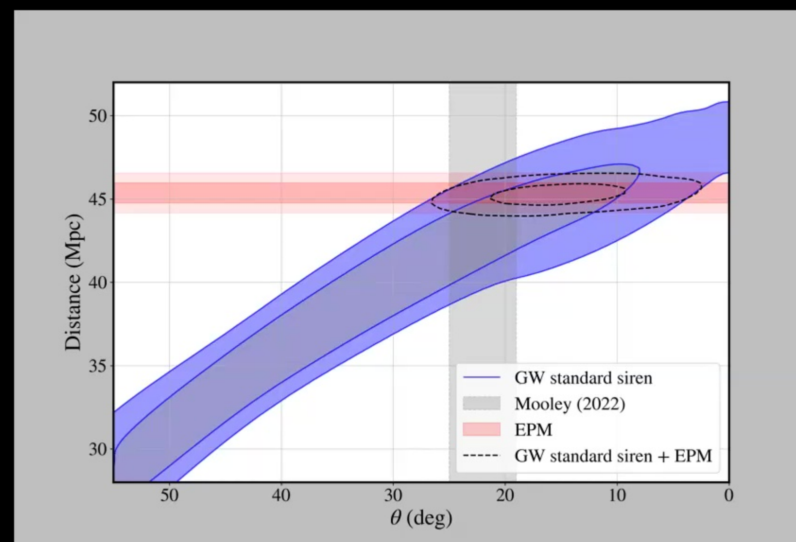

31

A Spherical Expansion - II

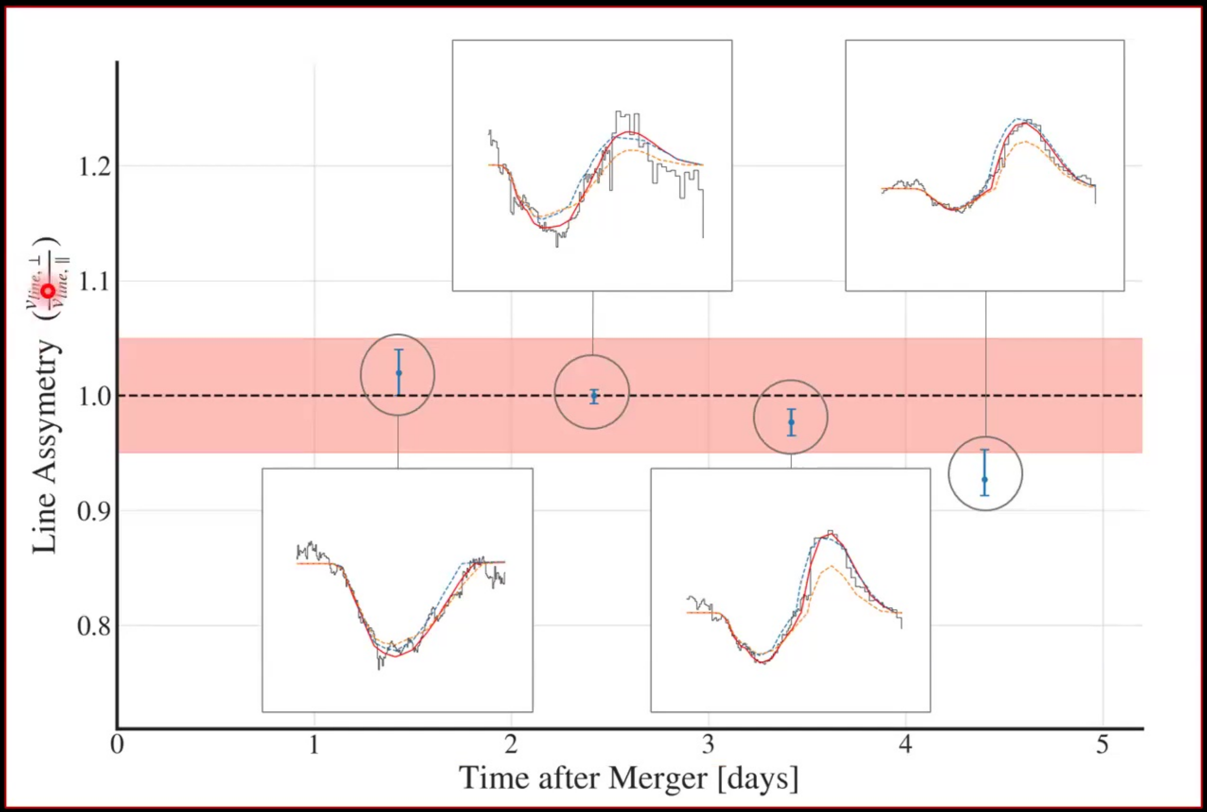

Sneppen, A.,Watson, D. et al (2023)

A Spherical Expansion - I + II

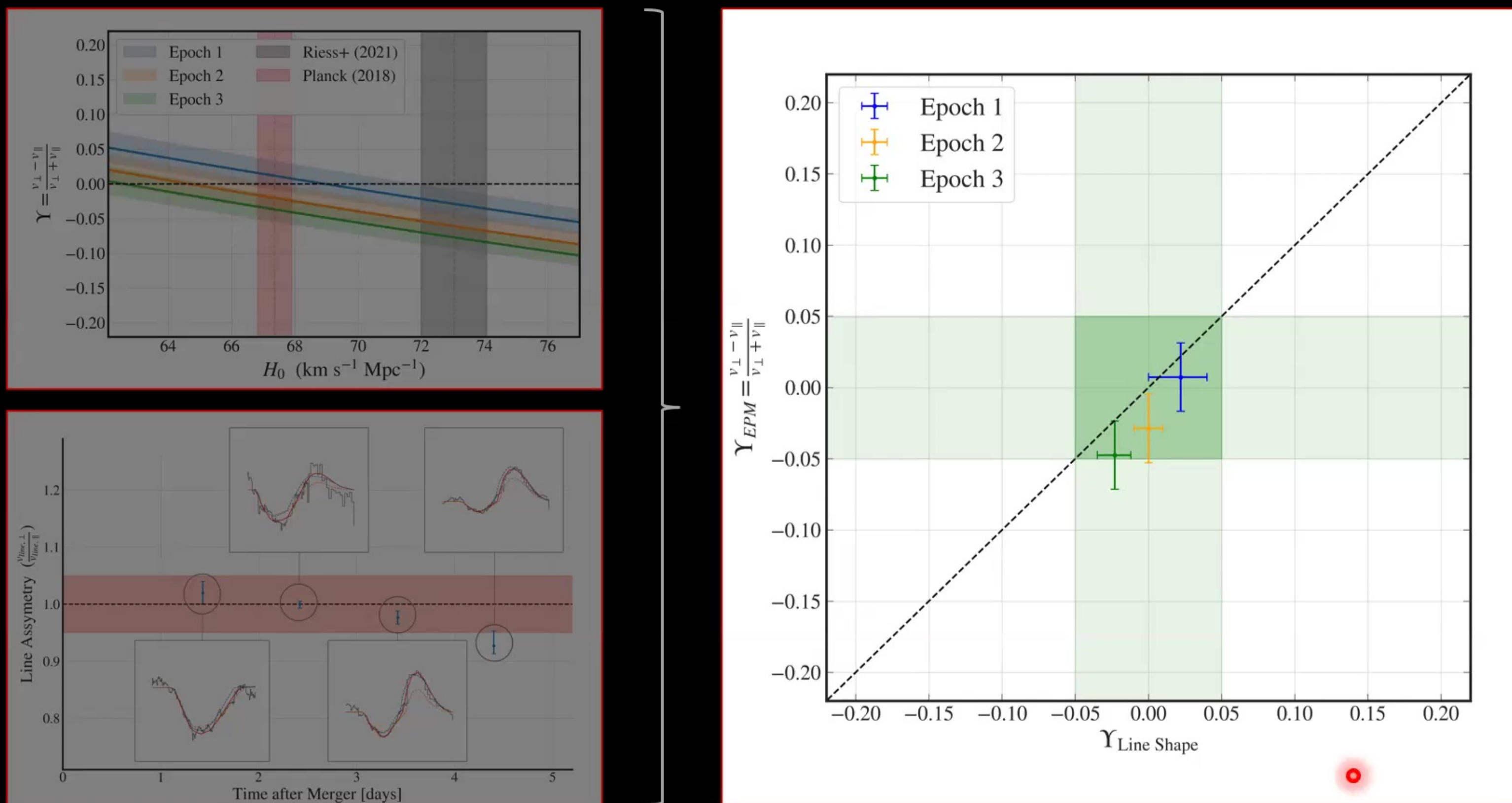

33

… and a few ongoing reflections

Line detection at ≈ 0.75 μm

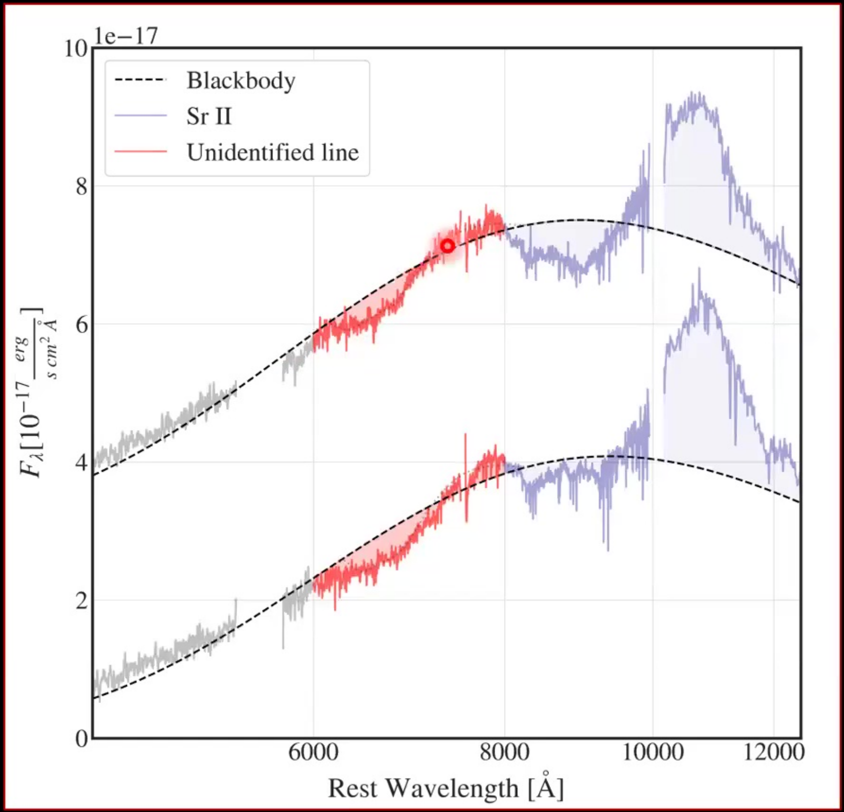

Sneppen and Watson, in prep, (2023)

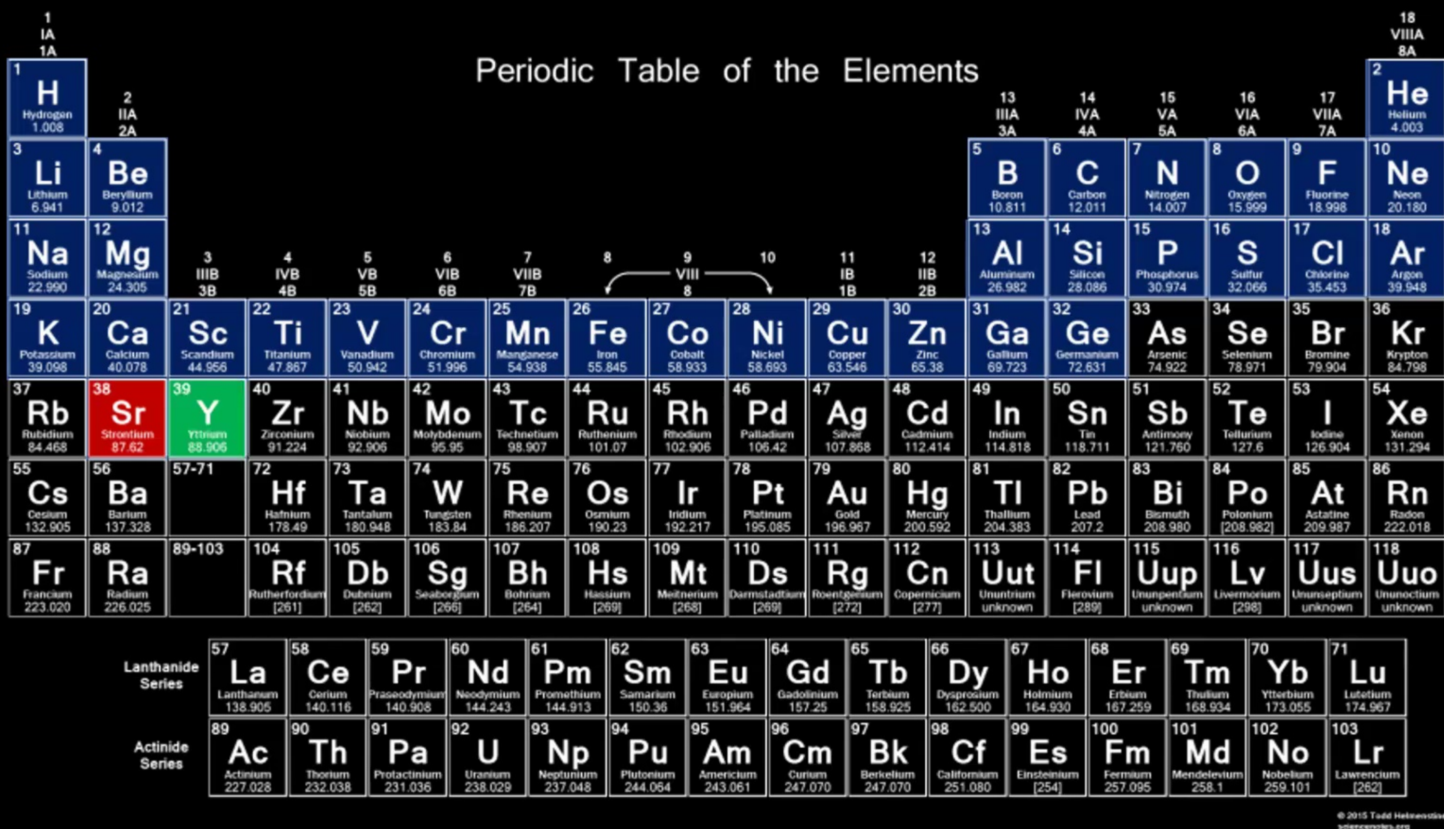
Periodic Table of the Elements
1 IA 1A
2 IIA 2A
3 IIIB 3B
4 IVB 4B
5 VB 5B
6 VIB 6B
7 VIIB 7B
8 9 VIII 8 10
11 IB 1B
12 IIB 2B
13 IIIA 3A
14 IVA 4A
15 VA 5A
16 VIA 6A
17 VIIA 7A
18 VIIIA 8A
1 H Hydrogen 1.008
2 He Helium 4.003
3 Li Lithium 6.941
4 Be Beryllium 9.012
5 B Boron 10.811
6 C Carbon 12.011
7 N Nitrogen 14.007
8 O Oxygen 15.999
9 F Fluorine 18.998
10 Ne Neon 20.180
11 Na Sodium 22.990
12 Mg Magnesium 24.305
13 Al Aluminum 26.982
14 Si Silicon 28.086
15 P Phosphorus 30.974
16 S Sulfur 32.066
17 Cl Chlorine 35.453
18 Ar Argon 39.948
19 K Potassium 39.098
20 Ca Calcium 40.078
21 Sc Scandium 44.956
22 Ti Titanium 47.867
23 V Vanadium 50.942
24 Cr Chromium 51.996
25 Mn Manganese 54.938
26 Fe Iron 55.845
27 Co Cobalt 58.933
28 Ni Nickel 58.693
29 Cu Copper 63.546
30 Zn Zinc 65.38
31 Ga Gallium 69.723
32 Ge Germanium 72.631
33 As Arsenic 74.922
34 Se Selenium 78.971
35 Br Bromine 79.904
36 Kr Krypton 84.798
37 Rb Rubidium 84.468
38 Sr Strontium 87.62
39 Y Yttrium 88.906
40 Zr Zirconium 91.224
41 Nb Niobium 92.906
42 Mo Molybdenum 95.95
43 Tc Technetium 98.907
44 Ru Ruthenium 101.07
45 Rh Rhodium 102.906
46 Pd Palladium 106.42
47 Ag Silver 107.868
48 Cd Cadmium 112.414
49 In Indium 114.818
50 Sn Tin 118.711
51 Sb Antimony 121.760
52 Te Tellurium 127.6
53 I Iodine 126.904
54 Xe Xenon 131.294
55 Cs Cesium 132.905
56 Ba Barium 137.328
57-71
72 Hf Hafnium 178.49
73 Ta Tantalum 180.948
74 W Tungsten 183.84
75 Re Rhenium 186.207
76 Os Osmium 190.23
77 Ir Iridium 192.217
78 Pt Platinum 195.085
79 Au Gold 196.967
80 Hg Mercury 200.592
81 Tl Thallium 204.383
82 Pb Lead 207.2
83 Bi Bismuth 208.980
84 Po Polonium [208.982]
85 At Astatine 209.987
86 Rn Radon 222.018
87 Fr Francium 223.020
88 Ra Radium 226.025
89-103
104 Rf Rutherfordium [261]
105 Db Dubnium [262]
106 Sg Seaborgium [266]
107 Bh Bohrium [264]
108 Hs Hassium [269]
109 Mt Meitnerium [268]
110 Ds Darmstadtium [269]
111 Rg Roentgenium [272]
112 Cn Copernicium [277]
113 Uut Ununtrium unknown
114 Fl Flerovium [289]
115 Uup Ununpentium unknown
116 Lv Livermorium [298]
117 Uus Ununseptium unknown
118 Uuo Ununoctium unknown
Lanthanide Series
57 La Lanthanum 138.905
58 Ce Cerium 140.116
59 Pr Praseodymium 140.908
60 Nd Neodymium 144.243
61 Pm Promethium 144.913
62 Sm Samarium 150.36
63 Eu Europium 151.964
64 Gd Gadolinium 157.25
65 Tb Terbium 158.925
66 Dy Dysprosium 162.500
67 Ho Holmium 164.930
68 Er Erbium 167.259
69 Tm Thulium 168.934
70 Yb Ytterbium 173.055
71 Lu Lutetium 174.967
Actinide Series
89 Ac Actinium 227.028
90 Th Thorium 232.038
91 Pa Protactinium 231.036
92 U Uranium 238.029
93 Np Neptunium 237.048
94 Pu Plutonium 244.064
95 Am Americium 243.061
96 Cm Curium 247.070
97 Bk Berkelium 247.070
98 Cf Californium 251.080
99 Es Einsteinium [254]
100 Fm Fermium 257.095
101 Md Mendelevium 258.1
102 No Nobelium 259.101
103 Lr Lawrencium [262]
© 2015 Todd Helmenstine
sciencenotes.org

Y^+ detection at $\approx 0.75\ \mu m$

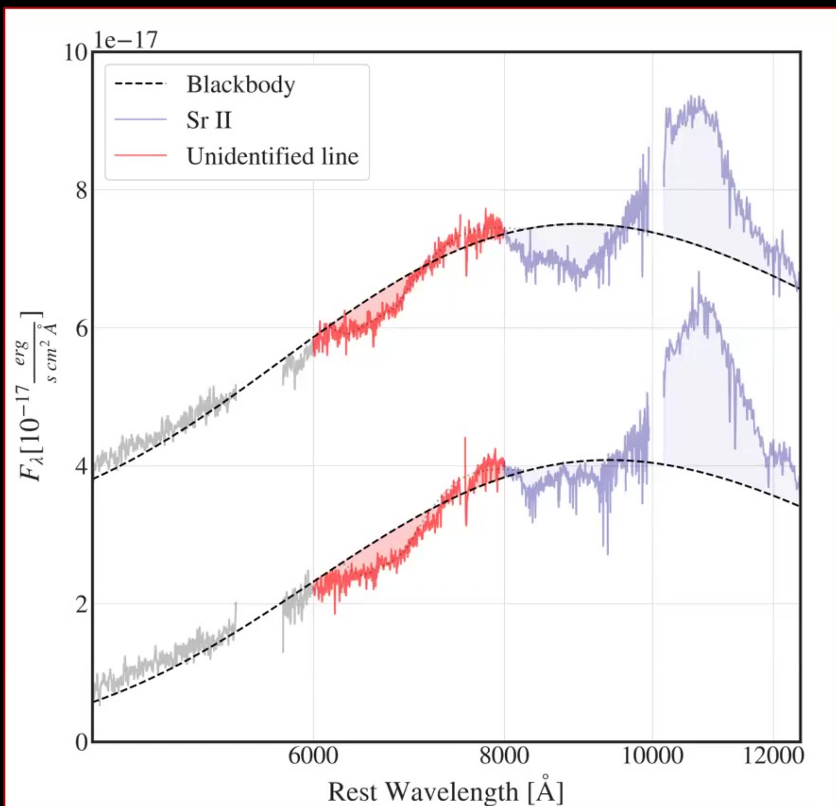

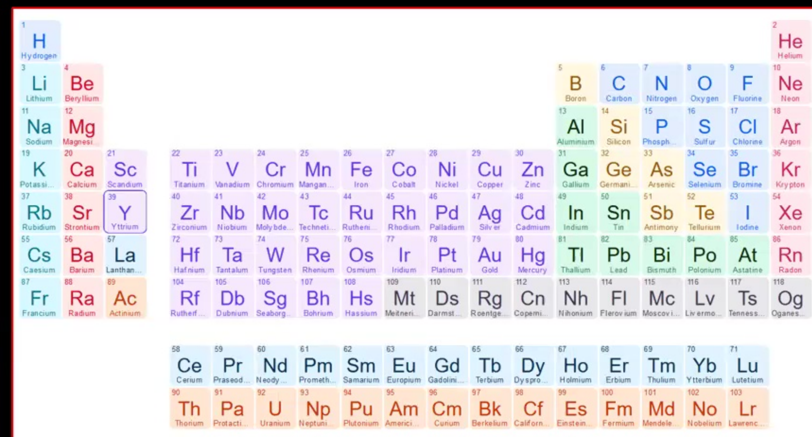

Table 2. Lines considered in the Y^+ P Cygni fits. Vacuum wavelengths (λ), energy levels (E), and oscillator strengths ($\log gf$) for Y^+ 4d5p to $4d^2$ line transitions are from Biémont et al. (2011).

λ	Lower level		Upper level		$\log gf$
(Å)	$4d^2$	E (cm^{-1})	4d5p	E (cm^{-1})	
7881.9	b^1D_2	14 832	$z^1P_1^\circ$	27 517	−0.60
7450.3	a^3P_2	14 098	$z^1P_1^\circ$	27 517	−1.44
7332.9	a^3P_0	13 883	$z^1P_1^\circ$	27 517	−1.98
7264.2	b^1D_2	14 832	$z^3D_1^\circ$	28 595	−1.11
6896.0	a^3P_2	14 098	$z^3D_1^\circ$	28 595	−1.67
6858.2	a^3P_1	14 018	$z^3D_1^\circ$	28 595	−1.69
6795.4	a^3P_0	13 883	$z^3D_1^\circ$	28 595	−1.54

Sneppen and Watson, in prep, (2023)

Models to Sphericity

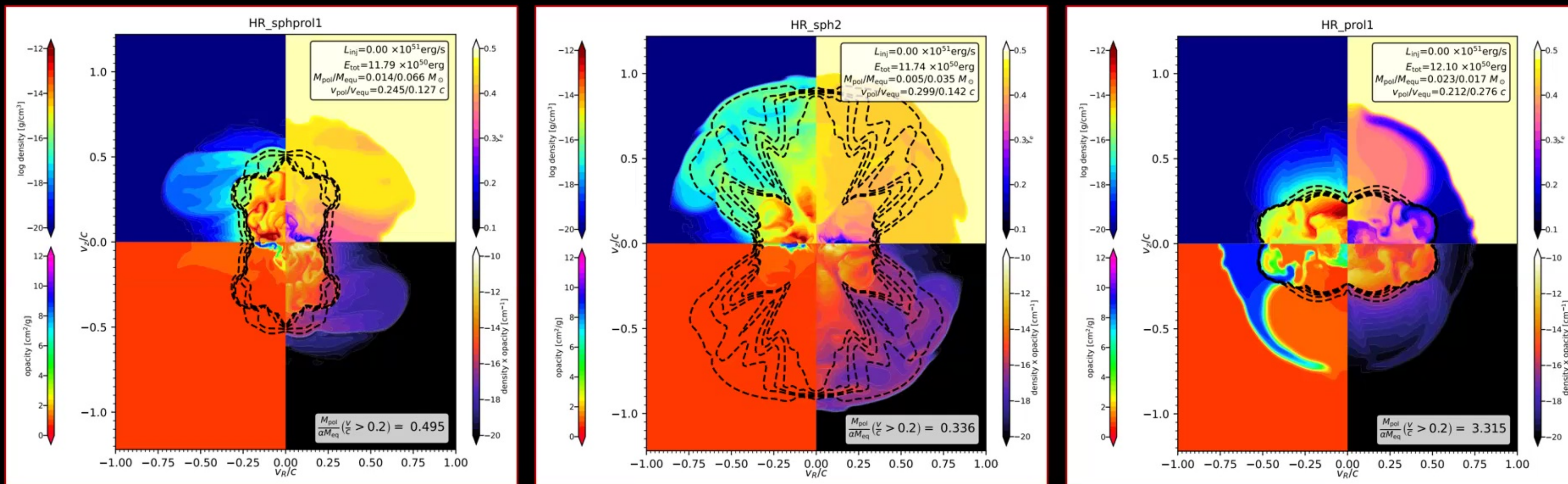

Produced by Oliver Just

41

An Outlook on H_0

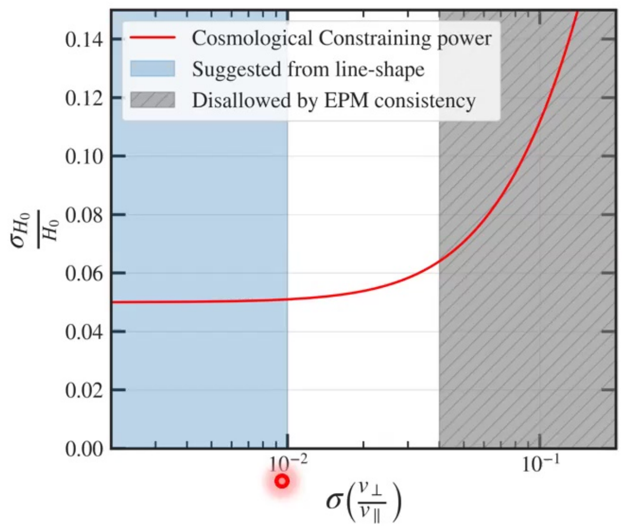

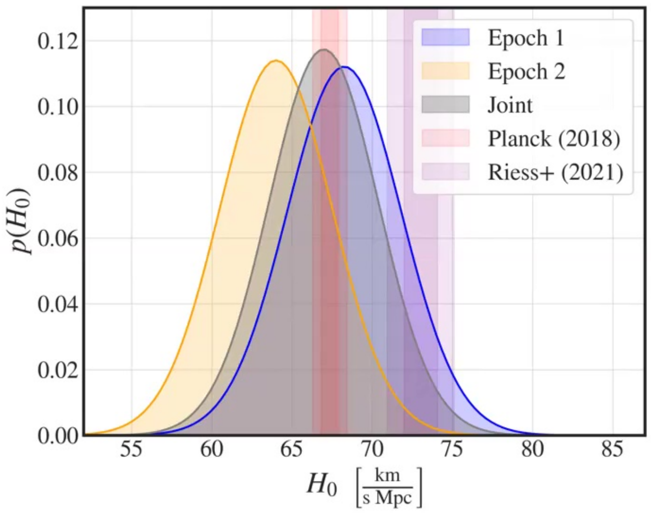

Sneppen, A.,Watson, D. et al, in prep, (2023)

An Outlook on H_0

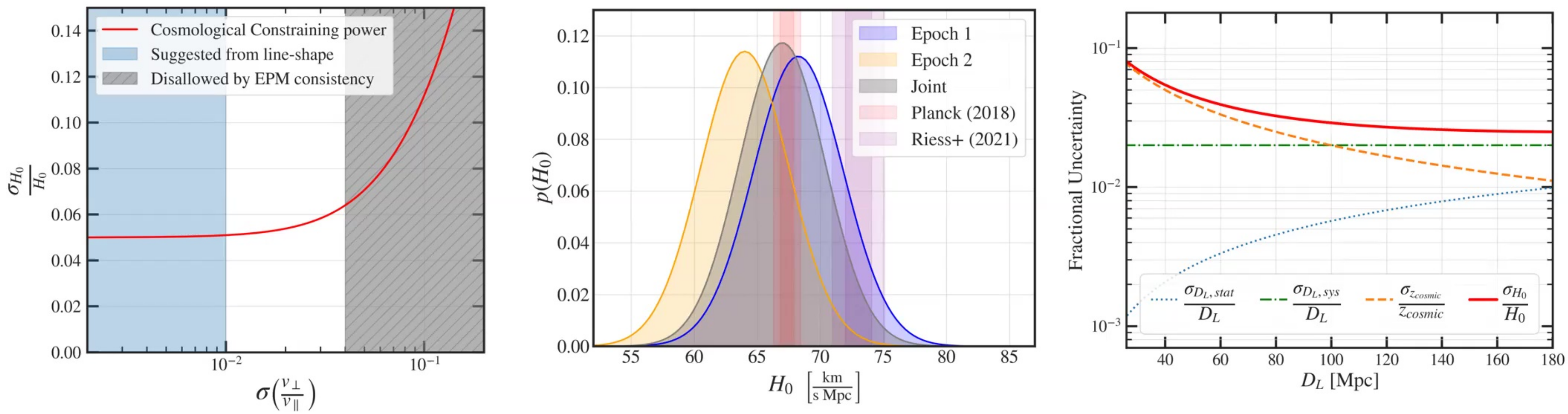

Sneppen, A.,Watson, D. et al, in prep, (2023)

Thank you for your attention

https://arxiv.org/abs/2302.06621

Article

Spherical symmetry in the kilonova AT2017gfo/GW170817

https://doi.org/10.1038/s41586-022-05616-x

Received: 12 July 2022

Accepted: 1 December 2022

[redacted]

Check for updates

Albert Sneppen[1,2]✉, Darach Watson[1,2], Andreas Bauswein[3], Oliver Just[3,4], Rubina Kotak[5], Ehud Nakar[6], Dovi Poznanski[6] & Stuart Sim[7]

The mergers of neutron stars expel a heavy-element enriched fireball that can be observed as a kilonova[1–4]. The kilonova's geometry is a key diagnostic of the merger and is dictated by the properties of ultra-dense matter and the energetics of the collapse to a black hole. Current hydrodynamical merger models typically show aspherical ejecta[5–7]. Previously, Sr^+ was identified in the spectrum[8] of the only well-studied kilonova[9–11] AT2017gfo[12], associated with the gravitational wave event GW170817. Here we combine the strong Sr^+ P Cygni absorption-emission spectral feature and the blackbody nature of kilonova spectrum to determine that the kilonova is highly spherical at early epochs. Line shape analysis combined with the known inclination angle of the source[13] also show the same sphericity independently. We conclude that energy injection by radioactive decay is insufficient to make the ejecta spherical. A magnetar wind or jet from the black-hole disk could inject enough energy to induce a more spherical distribution in the overall ejecta; however, an additional process seems necessary to make the element distribution uniform.